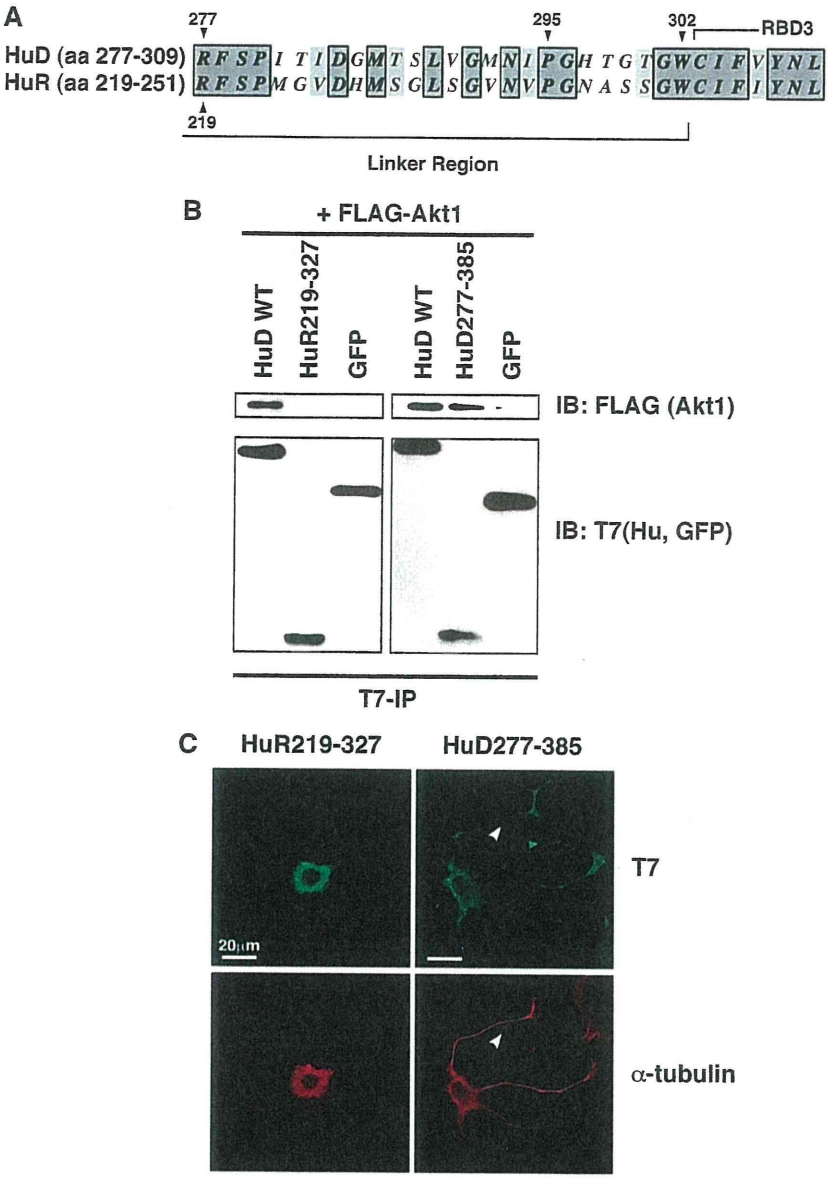

Figure 5. HuD 277-385 but not HuR 219-327 binds to Akt1 and induces neurite outgrowth in PC12 cells. (**A**) Amino acid alignment of the truncated linker and the start of the RBD3 sequence of the mutant HuD 277-385 (amino acids 277-309 is shown) and the mutant HuR 219-327 (amino acids 219-251 is shown). The amino acid sequence of HuD is compared with that of HuR. Identical residues are shown in gray. The linker region is indicated. (**B**) Specific coimmunoprecipitation of Akt1 with HuD 277-385 but not HuR 219-327. HeLa cells were transfected with the indicated constructs. Immunoprecipitated was performed with anti-T7 antibody. Coimmunoprecipitation was monitored by IB. GFP is a negative control. (**C**) HuD 277-385 but not HuR 219-327 induces neurite outgrowth in PC12 cells. Shown is the confocal analysis of PC12 cells that has been transfected with constructs coding for the indicated proteins. Cells were costained with anti-T7 (green) and with anti-α-tubulin antibody (red). Arrow heads point to induced neurites. Scale bar, 20 μm. The same results were obtained in at least three independent experiments.

performed an *in vitro* kinase reaction using GST-HuD and active Akt1 (see 'Materials and Methods' section for further details). The data shown in Figure 7 reveal that HuD is not phosphorylated by Akt1, whereas the positive control FOXO4 is. On the basis of these results, we conclude that HuD itself is not the target of Akt1. Taken together, with the results described above, our data suggest the model whereby RNA-bound HuD recruits Akt1 to activate neurite outgrowth.

DISCUSSION

Neuronal Hu proteins are RBPs that are critical for neuronal development (16). However, the underlying molecular mechanisms how neuronal Hu proteins exert their function are poorly understood. We have recently shown that HuD, a family member of neuronal proteins, stimulates cap- and poly(A)-dependent translation and found that the eIF4A and poly(A) binding

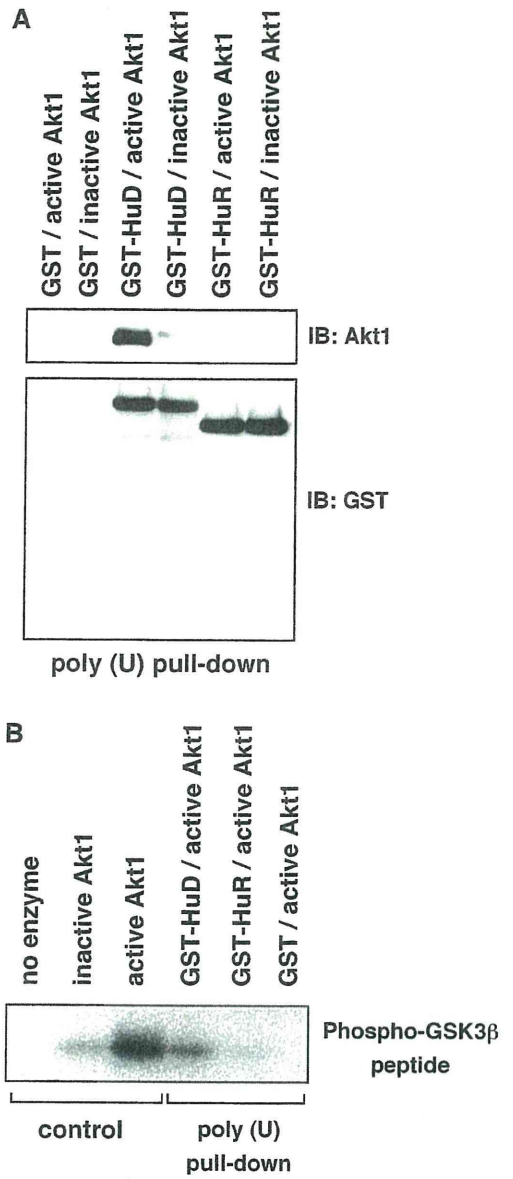

Figure 6. RNA-bound HuD interacts with active Akt1 and retains its kinase activity. (**A**) RNA-bound HuD interacts with active Akt1. Active or inactive Akt1 was incubated with GST, GST-HuD or GST-HuR, pulled down with poly(U)-sepharose beads and analyzed by IB and for pull-down efficiency (lower panel) by IB. (**B**) Akt1 retains its protein kinase activity in the Akt1–HuD–RNA complex. Active Akt1 was incubated with GST-HuD, GST-HuR or GST and then pulled down with poly(U)-sepharose beads. Protein kinase assays were performed using a GSK-3β peptide, which is a specific substrate for Akt1. Controls are standard assays with 'no enzyme', 'inactive Akt1' or 'active Akt1'. In the pull-down lanes approximately 10% of Akt1 has been used for the kinase assay as estimated by western blot analysis (data not shown).

domains which are key in this process also contribute to its neurite-inducing activity (4). Here, we further investigated the underlying molecular interactions and show that HuD directly and specifically interacts with active Akt1. This interaction is RNA independent, mediated by the linker region between RBD2 and RBD3 and required for its neurite inducing activity (Figures 2–5). We also tested for the interaction of HuD with downstream targets of Akt1 such as FLAG-mTOR or FLAG-S6K1 in HuD immunoprecipitates. However, we could not detect these downstream targets in the eluates (data not shown). Therefore, it appears that HuD interacts with Akt1 specifically and this interaction does not extend to other closely related AGC family kinases.

The strategy of an RBP to interact with a signaling pathway component has some similarity to that of the splicing factor 2 (SF2)/ASF which recruits mTOR or protein phosphatase 2A to activate translation of a subset of mRNAs (17). Interestingly, the finding that the eIF4A and poly(A) domains of HuD are not only critical for HuD's enhancer function in translation but also contribute to its neurite-inducing activity, strongly suggests that stimulation of translation is a prerequisite for the neurite inducing activity of HuD. This raises the possibility that the HuD–Akt1 interaction might underlie a function in regulating translation. eIF4A, which interacts with HuD (4), may help to recruit the HuD/Akt1 dimer into messenger ribonucleoprotein (mRNP) complexes to phosphorylate target molecules to stimulate translation.

What are the targets of Akt1 in such HuD-containing mRNP complexes? We found that HuD itself is not a direct target of Akt1 (Figure 7). A prime candidate target is eIF4B, which can be phosphorylated by Akt1 (Supplementary Figure S4) (18–20) and can stimulate the helicase activity of eIF4A (21,22) and as a consequence translation. Thus, eIF4A activity might indirectly be enhanced by the action of Akt1 kinase via phosphorylation of an activator of eIF4A (e.g. eIF4B) rather than directly, as eIF4A is known not to be phosphorylated. Future experiments will aim to directly address the question of whether tethered HuD enhances cap-dependent translation via regulating the phosphorylation status of eIF4B by recruiting Akt1 into translation mRNP complexes.

Taken together, our study uncovers a functional interaction between a key RBP involved in neuronal development and a key signaling molecule, which is a master modulator of translation. To our knowledge, this is the first demonstration of a signaling pathway kinase that is specifically recruited by an RBP to trigger neurite outgrowth. In addition, these data might help to explain how HuD enhances translation of mRNAs that encode proteins involved in neuronal development.

SUPPLEMENTARY DATA

Supplementary Data are available at NAR Online: Supplementary Figures S1–S4.

ACKNOWLEDGEMENTS

We thank Sven Danckwardt, Kent Duncan and Toshifumi Inada for comments on the manuscript and Yukiko Gotoh for kindly providing the Akt1 expression plasmid.

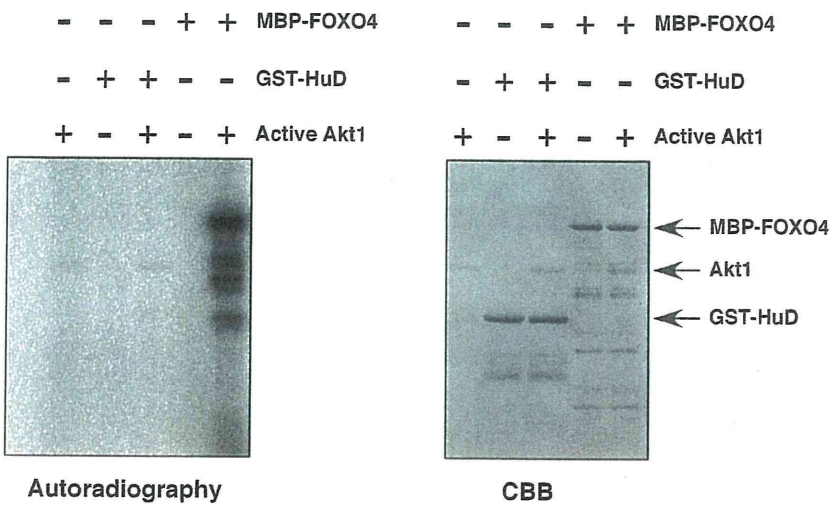

Figure 7. HuD is not a substrate of Akt1. *In vitro* kinase reaction using recombinant GST-HuD or MBP-FOXO4 and active Akt1 (see 'Material and Methods' section for further details). Phosphorylation levels are shown in the left panel, CBB stain is shown in the right panel. The positions of MBP-FOXO4, Akt1 and GST-HuD are indicated by arrows.

FUNDING

This work was supported by Grants-in-Aid from the Ministry of Education, Culture, Sports, Science and Technology of Japan (to T.F. and H.S.); Foundation NAGASE Science Technology Development (to T.F.). C.T. is a recipient of a Heisenberg-Fellowship from the Deutsche Forschungsgemeinschaft (DFG) (TH788/2-1 and TH788/2-2, to C.T.). Funding for open access charge: Intramural funding.

Conflict of interest statement. None declared.

REFERENCES

1. Jackson,R.J., Hellen,C.U. and Pestova,T.V. (2010) The mechanism of eukaryotic translation initiation and principles of its regulation. *Nat. Rev. Mol. Cell Biol.*, **11**, 113–127.
2. Sonenberg,N. and Hinnebusch,A.G. (2009) Regulation of translation initiation in eukaryotes: mechanisms and biological targets. *Cell*, **136**, 731–745.
3. Hinman,M.N. and Lou,H. (2008) Diverse molecular functions of Hu proteins. *Cell Mol. Life Sci.*, **65**, 3168–3181.
4. Fukao,A., Sasano,Y., Imataka,H., Inoue,K., Sakamoto,H., Sonenberg,N., Thoma,C. and Fujiwara,T. (2009) The ELAV protein HuD stimulates cap-dependent translation in a Poly(A)- and eIF4A-dependent manner. *Mol. Cell*, **36**, 1007–1017.
5. Vanhaesebroeck,B., Guillermet-Guibert,J., Graupera,M. and Bilanges,B. The emerging mechanisms of isoform-specific PI3K signalling. *Nat. Rev. Mol. Cell Biol.*, **11**, 329–341.
6. Crowder,R.J. and Freeman,R.S. (1998) Phosphatidylinositol 3-kinase and Akt protein kinase are necessary and sufficient for the survival of nerve growth factor-dependent sympathetic neurons. *J. Neurosci.*, **18**, 2933–2943.
7. Kasashima,K., Sakashita,E., Saito,K. and Sakamoto,H. (2002) Complex formation of the neuron-specific ELAV-like Hu RNA-binding proteins. *Nucleic Acids Res.*, **30**, 4519–4526.
8. Saito,K., Fujiwara,T., Katahira,J., Inoue,K. and Sakamoto,H. (2004) TAP/NXF1, the primary mRNA export receptor, specifically interacts with a neuronal RNA-binding protein HuD. *Biochem. Biophys. Res. Commun.*, **321**, 291–297.
9. Dudek,H., Datta,S.R., Franke,T.F., Birnbaum,M.J., Yao,R., Cooper,G.M., Segal,R.A., Kaplan,D.R. and Greenberg,M.E. (1997) Regulation of neuronal survival by the serine-threonine protein kinase Akt. *Science*, **275**, 661–665.
10. Kitamura,T., Ogawa,W., Sakaue,H., Hino,Y., Kuroda,S., Takata,M., Matsumoto,M., Maeda,T., Konishi,H., Kikkawa,U. *et al.* (1998) Requirement for activation of the serine-threonine kinase Akt (protein kinase B) in insulin stimulation of protein synthesis but not of glucose transport. *Mol. Cell Biol.*, **18**, 3708–3717.
11. Matsuzaki,H., Konishi,H., Tanaka,M., Ono,Y., Takenawa,T., Watanabe,Y., Ozaki,S., Kuroda,S. and Kikkawa,U. (1996) Isolation of the active form of RAC-protein kinase (PKB/Akt) from transfected COS-7 cells treated with heat shock stress and effects of phosphatidylinositol 3,4,5-trisphosphate and phosphatidylinositol 4,5-bisphosphate on its enzyme activity. *FEBS Lett.*, **396**, 305–308.
12. Matsuzaki,H., Ichino,A., Hayashi,T., Yamamoto,T. and Kikkawa,U. (2005) Regulation of intracellular localization and transcriptional activity of FOXO4 by protein kinase B through phosphorylation at the motif sites conserved among the FOXO family. *J. Biochem.*, **138**, 485–491.
13. Greene,L.A. and Tischler,A.S. (1976) Establishment of a noradrenergic clonal line of rat adrenal pheochromocytoma cells which respond to nerve growth factor. *Proc. Natl Acad. Sci. USA*, **73**, 2424–2428.
14. Vaudry,D., Stork,P.J., Lazarovici,P. and Eiden,L.E. (2002) Signaling pathways for PC12 cell differentiation: making the right connections. *Science*, **296**, 1648–1649.
15. Anderson,K.D., Morin,M.A., Beckel-Mitchener,A., Mobarak,C.D., Neve,R.L., Furneaux,H.M., Burry,R. and Perrone-Bizzozero,N.I. (2000) Overexpression of HuD, but not of its truncated form HuD I+II, promotes GAP-43 gene expression and neurite outgrowth in PC12 cells in the absence of nerve growth factor. *J. Neurochem.*, **75**, 1103–1114.
16. Deschenes-Furry,J., Perrone-Bizzozero,N. and Jasmin,B.J. (2006) The RNA-binding protein HuD: a regulator of neuronal differentiation, maintenance and plasticity. *Bioessays*, **28**, 822–833.
17. Michlewski,G., Sanford,J.R. and Caceres,J.F. (2008) The splicing factor SF2/ASF regulates translation initiation by enhancing phosphorylation of 4E-BP1. *Mol. Cell*, **30**, 179–189.
18. Raught,B., Peiretti,F., Gingras,A.C., Livingstone,M., Shahbazian,D., Mayeur,G.L., Polakiewicz,R.D., Sonenberg,N. and Hershey,J.W. (2004) Phosphorylation of eucaryotic translation

initiation factor 4B Ser422 is modulated by S6 kinases. *EMBO J.*, **23**, 1761–1769.
19. Shahbazian,D., Roux,P.P., Mieulet,V., Cohen,M.S., Raught,B., Taunton,J., Hershey,J.W., Blenis,J., Pende,M. and Sonenberg,N. (2006) The mTOR/PI3K and MAPK pathways converge on eIF4B to control its phosphorylation and activity. *EMBO J.*, **25**, 2781–2791.
20. van Gorp,A.G., van der Vos,K.E., Brenkman,A.B., Bremer,A., van den Broek,N., Zwartkruis,F., Hershey,J.W., Burgering,B.M., Calkhoven,C.F. and Coffer,P.J. (2009) AGC kinases regulate phosphorylation and activation of eukaryotic translation initiation factor 4B. *Oncogene*, **28**, 95–106.
21. Rozen,F., Edery,I., Meerovitch,K., Dever,T.E., Merrick,W.C. and Sonenberg,N. (1990) Bidirectional RNA helicase activity of eucaryotic translation initiation factors 4A and 4F. *Mol. Cell Biol.*, **10**, 1134–1144.
22. Altmann,M., Muller,P.P., Wittmer,B., Ruchti,F., Lanker,S. and Trachsel,H. (1993) A Saccharomyces cerevisiae homologue of mammalian translation initiation factor 4B contributes to RNA helicase activity. *EMBO J.*, **12**, 3997–4003.

THE JOURNAL OF BIOLOGICAL CHEMISTRY VOL. 287, NO. 15, pp. 11924–11933, April 6, 2012

Double Plant Homeodomain (PHD) Finger Proteins DPF3a and -3b Are Required as Transcriptional Co-activators in SWI/SNF Complex-dependent Activation of NF-κB RelA/p50 Heterodimer*[S]

Received for publication, November 10, 2011, and in revised form, January 30, 2012 Published, JBC Papers in Press, February 13, 2012, DOI 10.1074/jbc.M111.322792

Aya Ishizaka[‡1], Taketoshi Mizutani[‡§], Kazuyoshi Kobayashi[‡], Toshio Tando[‡], Kouhei Sakurai[‡], Toshinobu Fujiwara[¶], and Hideo Iba[‡2]

From the [‡]Division of Host-Parasite Interaction, Department of Microbiology and Immunology, Institute of Medical Science, University of Tokyo, 4-6-1 Shirokanedai, Minato-ku, Tokyo 108-8639, [§]RNA and Biofunctions, PRESTO, Japan Science and Technology Agency, 4-1-8 Honcho, Kawaguchi, Saitama 332-0012, and the [¶]Institute of Microbial Chemistry Laboratory of Disease Biology, 3-14-23 Kamiosaki, Shinagawa-ku, Tokyo 141-0021, Japan

Background: The NF-κB dimer, RelA/p50, often requires the SWI/SNF complex for its transactivation function, but its molecular mechanisms remain elusive.
Results: The NF-κB canonical pathway induced by TNF-α is DPF3a/b- and SWI/SNF-dependent for some promoters.
Conclusion: DPF3a and DPF3b are effective linkers for the SWI/SNF complex and RelA/p50.
Significance: The NF-κB·DPF3a/b·SWI/SNF complex would be an effective platform for promoter-specific transactivation.

We have previously shown that DPF2 (requiem/REQ) functions as a linker protein between the SWI/SNF complex and RelB/p52 NF-κB heterodimer and plays important roles in NF-κB transactivation via its noncanonical pathway. Using sensitive 293FT reporter cell clones that had integrated a SWI/SNF-dependent NF-κB reporter gene, we find in this study that the overexpression of DPF1, DPF2, DPF3a, DPF3b, and PHF10 significantly potentiates the transactivating activity of typical NF-κB dimers. Knockdown analysis using 293FT reporter cells that endogenously express these five proteins at low levels clearly showed that DPF3a and DPF3b, which are produced from the *DPF3* gene by alternative splicing, are the most critical for the RelA/p50 NF-κB heterodimer transactivation induced by TNF-α stimulation. Our data further show that this transactivation requires the SWI/SNF complex. DPF3a and DPF3b are additionally shown to interact directly with RelA, p50, and several subunits of the SWI/SNF complex *in vitro* and to be co-immunoprecipitated with RelA/p50 and the SWI/SNF complex from the nuclear fractions of cells treated with TNF-α. In ChIP experiments, we further found that endogenous DPF3a/b and the SWI/SNF complex are continuously present on HIV-1 LTR, whereas the kinetics of RelA/p50 recruitment after TNF-α treatment correlate well with the viral transcriptional activation levels. Additionally, re-ChIP experiments showed DPF3a/b and the SWI/SNF complex associate with RelA on the endogenous *IL-6* promoter after TNF-α treatment. In conclusion, our present data indicate that by linking RelA/p50 to the SWI/SNF complex, DPF3a/b induces the transactivation of NF-κB target gene promoters in relatively inactive chromatin contexts.

NF-κB[3] is a key transcription factor that regulates many biological processes, such as immune, inflammatory, and virus responses, development, cellular growth, and apoptosis. The regulation by NF-κB is achieved through the transactivation of a large number of its target genes in a cell type-specific and/or stimulus-specific manner (1–4). NF-κB is itself composed of homo- or heterodimeric complexes of members of the NF-κB family of proteins, which include RelA (p65), RelB, c-Rel, p50, and p52 in humans. NF-κB dimers remain inactive in the cytoplasm until specific stimulation activates their signaling pathways (5). One of the main NF-κB pathways, the canonical pathway, is triggered by stimulation with factors such as tumor necrosis factor-α (TNF-α) and lipopolysaccharide (LPS). The induction of this pathway results in the activation of the RelA/p50 heterodimer by transporting it to the nucleus after phosphorylation and also the proteasomal degradation of inhibitor of NF-κB (IκB), which retains RelA/p50 in the cytoplasm under unstimulated conditions (6). However, RelB/p52, which is present in the cytoplasm as inactive RelB/p100 (NF-κB1) until stimulated, is activated through the noncanonical pathway (7). This pathway is triggered by stimuli such as lymphotoxin exposure, and it induces the cleavage of cytosolic p100 to produce p52, which subsequently translocates into the nucleus as a RelB/p52 dimer.

* This work was supported by Grants-in-aid for Scientific Research on Priority Areas 17016015 and for Scientific Research (B) 22300318 and (C) 21590507 from the Ministry of Education, Culture, Sports, Science and Technology, Japan, and by a grant from the Japan Society for the Promotion of Science.
[S] This article contains supplemental Figs. S1-S9, Table S1, and experimental procedures.
[1] Research Fellow of the Japan Society for the Promotion of Science.
[2] To whom correspondence should be addressed: Division of Host-Parasite Interaction, Dept. of Microbiology and Immunology, Institute of Medical Science, University of Tokyo, 4-6-1 Shirokanedai, Minato-ku, Tokyo 108-8639, Japan. Tel.: 81-3-5449-5730; Fax: 81-3-5449-5449; E-mail: iba@ims.u-tokyo.ac.jp.

[3] The abbreviations used are: NF-κB, nuclear factor-κB; PHD, plant homeodomain; Luc, luciferase.

The mechanism by which each NF-κB dimer is recruited to a certain set of promoters and specifically transactivates their transcription in a cell type-dependent manner is an important question. Such processes would likely involve chromatin context-dependent regulation. Indeed, NF-κB transactivation is known to often require the SWI/SNF complex, a representative chromatin remodeling factor involved in epigenetic regulation in humans, but no clear and direct interaction between NF-κB components and the SWI/SNF complex has been reported. The SWI/SNF complex has two alternative ATPases, Brahma (Brm) or Brahma-related gene 1 (BRG1) as the catalytic subunits, and other subunits such as BAF155, Ini1/SNF5, BAF170, BAF60a, and β-actin (8–10). The SWI/SNF complex is recruited to target genes via association with transcription regulators such as c-Myc (11), C/EBPβ (12), AP-1 (13), neuron-restrictive silencer factor (14), and Cdx2 (15). In addition to cellular targets, we have shown that integrated LTRs of murine leukemia virus (16, 17) and HIV-1 (human immunodeficiency virus-1) (18) require the Brm-type SWI/SNF complex to maintain their gene expression.

We have recently shown that DPF2 (REQ/BAF45d) functions as an efficient adaptor protein between the SWI/SNF complex and RelB/p52 and plays important roles in NF-κB transcriptional activation at the most downstream part of the NF-κB noncanonical pathway (19). DPF2 belongs to the d4 family of proteins, the members of which are characterized by an N-terminal 2/3 domain containing a nuclear localization signal, a central C2H2-type Krüppel-like zinc finger motif, and a C-terminal d4 domain consisting of a tandem repeat of the PHD zinc finger (20–22). It was previously shown that another member of the d4 family, DPF3 (Cerd4/BAF45c), associates with the SWI/SNF complex and further that the *DPF3* gene has two splicing variants, the products of which differ at their C-terminal regions. The DPF3b protein shows all of the characteristics of a d4 family member, including binding activity to either methylated or acetylated lysine residues at histones H3 and H4 through the PHD fingers. However, DPF3a lacks these binding activities as it harbors a truncated d4 domain within its first PHD (23). Interestingly, two d4 family members, DPF1 (Neud4/BAF45b) and DPF3, and an additional protein, PHF10 (BAF45a), which also possesses double PHD fingers within its C terminus, have been reported to associate with the SWI/SNF complex in neural cells in a differentiation-specific manner (24). In mouse neural progenitors, the complex contains PHF10, but this component is substituted by DPF1 or DPF3 when the cells become differentiated into post-mitotic neurons.

Considering our previous finding that DPF2 is required for RelB/p52 transactivation via the SWI/SNF complex, we speculate that the five proteins DPF1, DPF2, DPF3a, DPF3b, and PHF10 are candidate co-activators of the typical NF-κB heterodimer, RelA/p50, as well as two other NF-κB dimers, RelB/p52 and c-Rel/p50. We show in our current analysis that each of these proteins can enhance the different NF-κB heterodimers to transactivate their targets efficiently when both they and the NF-κB components are exogenously expressed. We further show from our analysis that among these five proteins DPF3a and DPF3b are the most effective cofactors for RelA/p50 activation in 293FT cells treated with TNF-α. Our current data further indicate that these two proteins directly bind to RelA, p50, and at least four subunits of the SWI/SNF complex *in vitro*. We additionally show that endogenous DPF3a/b and the SWI/SNF complex are continuously co-localized at the HIV-1 LTR throughout the period of TNF-α stimulation and that RelA/p50 is promptly recruited to the typical NF-κB-binding sites within the HIV-1 LTR or endogenous *IL-6* promoter upon stimulation. Finally, we show that the viral transcripts are synthesized with similar kinetics to those of RelA/p50 recruitment.

EXPERIMENTAL PROCEDURES

Cell Culture and Retro- and Lentiviral Vectors—293FT cells (Invitrogen) were maintained in Dulbecco's modified Eagle's medium (Wako Chemicals, Tokyo) containing 10% fetal calf serum at 37 °C and 5% CO_2. For TNF-α stimulation, the cells were treated with 10 ng/ml TNF-α (R&D Systems, Minneapolis, MN). Vesicular stomatitis virus G protein (VSV-G)-pseudotyped retro- or lentiviral vectors were prepared as described previously (17, 19). For transduction, cells were incubated with the virus vector stocks in the presence of 8 μg/ml Sequabrene™ (Sigma).

Antibodies—Rabbit polyclonal antibodies against human DPF3 were raised against a synthetic peptide corresponding to amino acid residues 230–251 of the protein (NP_036206) by Medical and Biological Laboratories (MBL, Nagoya, Japan). Other antibodies used in this research are as follows: normal rabbit IgG (PM035) (MBL), α-RelA (C-20), α-BRG-1 (H-88), α-BAF155 (H-76) (Santa Cruz Biotechnology, Santa Cruz, CA), α-p105/p50 (ab7971), α-Brm (ab15597) (Abcam, Cambridge, MA), α-FLAG (M2) (Sigma), α-BAF60a (611728), and α-Ini1 (612110) (BD Transduction Laboratories, San Jose, CA). Most of these specific antibodies are rabbit polyclonal, except α-FLAG, α-BAF60a, and α-Ini1 which are mouse monoclonal.

GST Fusion Protein Pulldown Assays—GST fusion proteins were expressed in *Escherichia coli* Rosetta 2 (Novagen, Madison, WI) via incubation of the cells with 0.1 mM isopropyl 1-thio-β-D-galactopyranoside overnight at 15 °C and then prepared using His tag Binding/Wash Buffer (20 mM Tris-HCl (pH 8.0), 600 mM NaCl, 1 mM $MgCl_2$, 10% glycerol, 0.1% Nonidet P-40, 20 mM imidazole, and phosphatase inhibitors). Purification of GST-His-tagged proteins was performed sequentially using Profinity IMAC nickel-charged resin (Bio-Rad) and glutathione-Sepharose 4B (GE Healthcare). The target proteins were eluted from these columns with His tag Elution Buffer (20 mM Tris-HCl (pH 8.0), 600 mM NaCl, 1 mM $MgCl_2$, 10% glycerol, 0.1% Nonidet P-40, 250 mM imidazole, and phosphatase inhibitors) and GST Elution Buffer (100 mM Tris-HCl (pH 8.0), 12 mM NaCl, 20 mM glutathione, and phosphatase inhibitors), respectively. *In vitro* transcription and translation were then performed as described previously (19). *In vitro* synthesized proteins were incubated with respective GST fusion proteins for 2 h at 4 °C on a rotating platform. The complexes were washed for five times with TNE buffer (10 mM Tris-HCl (pH 7.8), 150 mM NaCl, 1 mM EDTA, 1% Nonidet P-40, and protease inhibitors) and analyzed by SDS-PAGE followed by autoradiography using FLA-5100 (Fujifilm). Cellular lysates, prepared in TN buffer (10 mM Tris-HCl (pH 7.8), 150 mM NaCl, 1% Nonidet P-40, protease inhibitors, and phosphatase inhibitors) were

treated with 100 units/ml benzonase endonuclease (Novagen) and precleared by incubation with GST protein immobilized on beads for 1 h. The lysate was then incubated with respective GST fusion proteins for 4 h at 4 °C on a rotating platform. The complexes were subsequently washed three times with Buffer D (20 mM HEPES-KOH (pH 7.9), 20% glycerol, 0.1 M KCl, 0.2 mM EDTA, 0.1% Nonidet P-40, and protease inhibitors) and analyzed by immunoblotting.

Chromatin Immunoprecipitation (ChIP) and Sequential ChIP Assays—Cells were cross-linked with 1% formaldehyde at 37 °C for 8 min. Cross-linking reactions were stopped by the addition of a 0.1 volume of 1.5 M glycine and incubation at room temperature for 5 min. The cells were then washed with PBS, collected, and incubated in lysis buffer 1 (50 mM HEPES (pH 7.5), 140 mM NaCl, 1 mM EDTA, 10% glycerol, 0.5% Nonidet P-40, 0.25% Triton X-100, and protease inhibitors). Cell lysates were sequentially replaced with lysis buffer 2 (10 mM Tris-HCl (pH 8.0), 200 mM NaCl, 1 mM EDTA, 0.5 mM EGTA, and protease inhibitors), and lysis buffer 3 (10 mM Tris-HCl (pH 8.0), 300 mM NaCl, 1 mM EDTA, 0.5 mM EGTA, 0.1% sodium deoxycholate, 0.5% *N*-lauroylsarcosine, and protease inhibitors). The lysates were then sonicated using Elestein Ryuseikai (Elekon Science. Corp., Chiba, Japan) on ice so that the DNA would be sheared into small fragments with an average length of less than 0.5 kb. After the addition of a 0.1 volume of 10% Triton X-100, the lysates were centrifuged to remove cellular debris and incubated overnight on a rotating platform at 4 °C with the respective antibodies (10 μg of each), which were previously bound to Dynabeads protein G (Invitrogen). The beads were washed once in low salt buffer (20 mM Tris-HCl (pH 8.0), 150 mM NaCl, 2 mM EDTA, 0.1% SDS, 1% Triton X-100, and protease inhibitors), twice in high salt buffer (20 mM Tris-HCl (pH 8.0), 400 mM NaCl, 2 mM EDTA, 0.1% SDS, 1% Triton X-100, and protease inhibitors), five times in RIPA buffer (50 mM HEPES (pH 7.6), 500 mM LiCl, 1 mM EDTA, 0.1% SDS, 1% Triton X-100, and protease inhibitors), and once in a TE, 50 mM NaCl buffer. The immune complexes were harvested in elution buffer (10 mM Tris-HCl (pH 7.5), 1 mM EDTA, 1% SDS and 100 mM DTT). For re-ChIP assays, the eluted complexes were diluted 1:10 with dilution buffer (10 mM Tris-HCl (pH 7.5), 150 mM NaCl, 1 mM EDTA, 0.5% sodium deoxycholate, 1% Nonidet P-40, and protease inhibitors), and the steps of ChIP assay were repeated. Cross-linking was reversed by incubation overnight at 65 °C with a 0.04 volume of 5 M NaCl. After treatment with proteinase K (Wako), the DNA was purified using Nucleospin Extract II (Macherey-Nagel, Düren, Germany) and quantified by real time PCR on a 7300 Real Time PCR System (Applied Biosystems, Bedford, MA) using Premix Ex Taq (Probe qPCR) or SYBR Premix Ex Taq (Takara Bio, Shiga, Japan). The specific primer pairs and probes used in this study are listed in supplemental Table S1.

Other Procedures—Details of the materials and methods used in this study can be found in the supplemental experimental procedures.

RESULTS

High Expression of Each Member of the d4 Family and PHF10 Enhances the Transactivating Activity of RelA/p50, RelB/p52, and c-Rel/p50—We previously generated a 293FT cell line stably harboring an exogenous expression unit composed of tandem NF-κB-responsive elements, a minimum promoter (MinP), and the downstream luciferase (Luc) reporter gene (293FT-NF-κB-MinP-Luc) (Fig. 1*A*) (Ref 19), in which the NF-κB-binding sites were derived from HIV-1 LTR (Fig. 1*B*). Whereas this reporter cell system was useful in evaluating chromosome structure-dependent NF-κB transactivation, it was found not to be as sensitive in responding to the exogenous introduction of NF-κB. We thus isolated several additional cellular clones from this parental reporter cell population and tested each for Luc inducibility following TNF-α treatment. A clone, which we designated as 293FT-NF-κB-MinP-Luc-A3, (abbreviated as NF-κB-MinP-Luc-A3 hereafter), showed one of the highest levels of Luc inducibility by TNF-α and was selected for further analysis (supplemental Fig. S1).

Expression vectors for the five co-activator candidate proteins, four d4 family proteins and PHF10 (supplemental Fig. S2), as well as the empty vector (CV-1) as a control were transfected into NF-κB-MinP-Luc-A3 together with each pair of plasmids expressing the NF-κB dimer, RelA/p50, RelB/p52, or c-Rel/p50, as well as the control vector for NF-κB expression (CV-2). The expression of these five candidate proteins that were tagged with FLAG at their N termini were confirmed by immunoblotting (supplemental Fig. S3*A*). As shown in Fig. 1*C*, the basal Luc activity in cells transfected with CV-2 was not significantly affected by the introduction of any of the candidate proteins (*lanes 2–6* compared with *lane 1*). Compared with the Luc activity of cells transfected with CV-1, the introduction of RelA/p50, RelB/p52, and c-Rel/p50 increased these reporter expression levels by 42-, 6-, and 3-fold, respectively (Fig. 1*C*, *lanes 13, 19,* and *7* compared with *lane 1*). These results indicated that NF-κB-MinP-Luc-A3 has very low basal NF-κB activity and that none of the candidates have any effects alone under these conditions, even if expressed at high levels. Importantly, transactivation mediated through RelA/p50 (Fig. 1*C*, *lanes 14–18* compared with *lane 13*), RelB/p52 (*lanes 20–24* compared with *lane 19*), and c-Rel/p50 (*lanes 8–12* compared with *lane 7*) was enhanced by the endogenous expression of any of the five candidate proteins (*lanes 7–24*). No significant differences were found among these five proteins in terms of the enhancement of any of the three NF-κB dimers, suggesting that all potentially function as co-activators of NF-κB in any context, at least when expressed at high levels.

Both DPF3a and DPF3b Are Required for SWI/SNF-dependent Transcriptional Activation through the NF-κB Canonical Pathway—We concluded that transfection experiments involving NF-κB expression vectors would not fully reflect NF-κB activation induced by naturally occurring signal transduction pathways and that the transient expression of candidate proteins by plasmid vectors is very high and thus far from physiological (supplemental Fig. S4). Hence, the experimental conditions used above would most likely not reflect the functional specificity of these proteins correctly. We thus examined the requirement for each candidate protein in the activation of NF-κB by TNF-α treatment, which strongly and almost exclusively activates the endogenous RelA/p50 dimer. Because 293FT cells express all of the transcripts coding these five can-

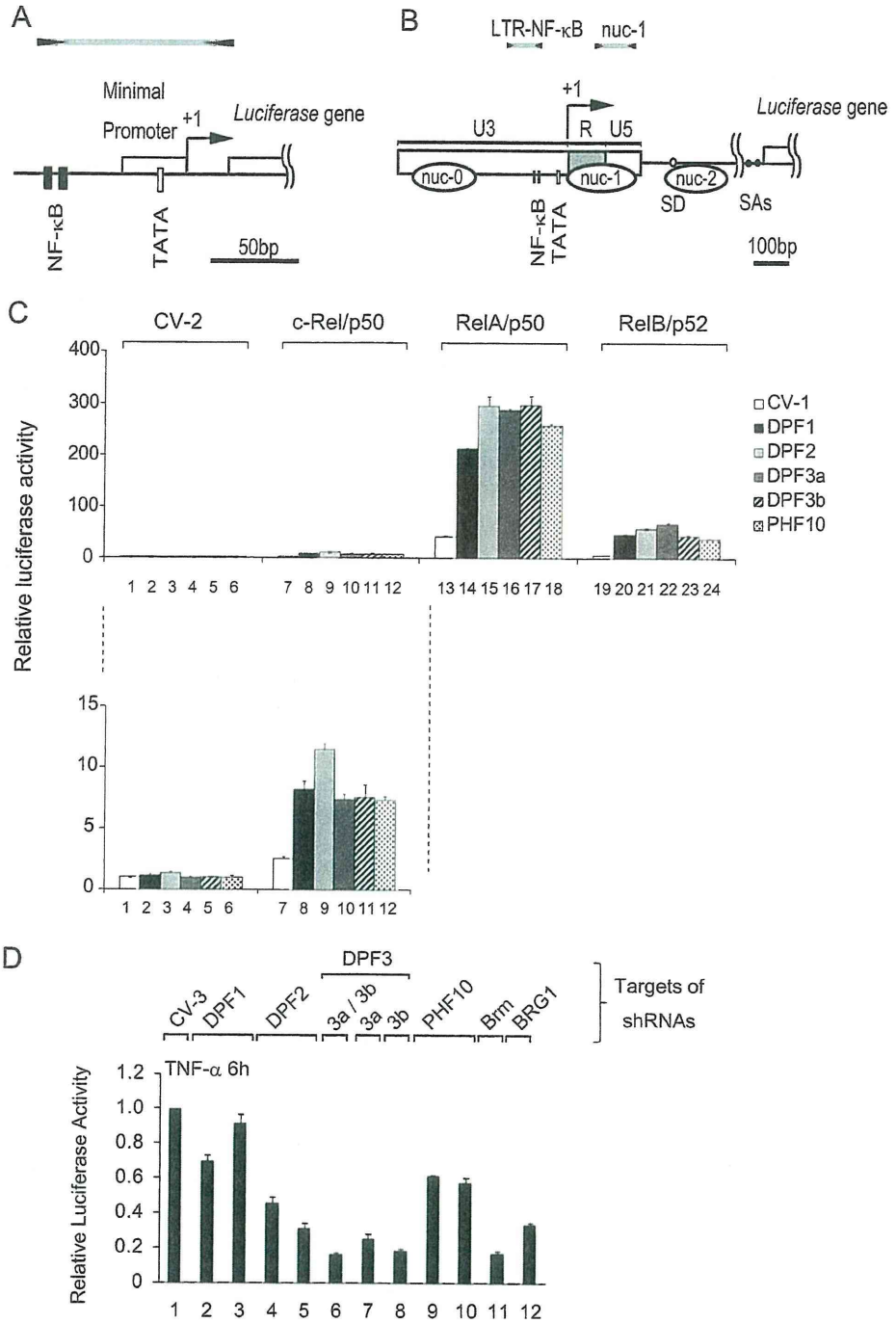

FIGURE 1. **d4 family members are potentially involved in both the canonical and noncanonical NF-κB transactivation of SWI/SNF-dependent promoters.** *A* and *B*, schematic representation of the constructs used in this study: NF-κB-MinP (*A*) and HIV-1 LTR (*B*). The binding sites for NF-κB and the TATA boxes are highlighted by *black* and *white bars*, respectively. Transcriptional start sites are designated as +1. Positions detected by real time PCR are indicated by *black arrows* and *gray bars*. The splicing donor and the acceptors are indicated by *white* and *black circles*. *C*, NF-κB-MinP-Luc-A3 cells were cotransfected with 10 ng of vectors expressing NF-κB subunits and 490 ng of candidate protein expressing or respective control vectors in different combinations. Luciferase activity was measured 48 h after transfection and normalization using control plasmid transfectants. *D*, NF-κB-MinP-Luc-A3 cells were transfected with 500 ng of vectors expressing short hairpin RNAs against each candidate protein and also *Brm* or *BRG1*. At 42 h post-transfection, cells were treated with 10 ng/ml TNF-α for 6 h, which led to a 1500-fold activation of luciferase activity compared with the control vector (CV-3) transfectants (data not shown). Luciferase activities were normalized to the CV-3 control transfectants. The corresponding target sites of the shRNAs against each of the candidates analyzed in this experiment are shown in supplemental Fig. S1. *Lane 2*, shDPF1-cds-1; *lane 3*, shDPF1-utr-1; *lane 4*, shREQ#1; *lane 5*, shREQ#2; *lane 6*, shDPF3-cds-1; *lane 7*, shDPF3a-utr-2; *lane 8*, shDPF3b-cds-3; *lane 9*, shPHF10-cds-1; and *lane 10*, shPHF10-utr-1. The results presented here are the average of at least three independent experiments, and the *bars* indicate the standard deviation.

didate proteins, as judged by semi-quantitative RT-PCR (supplemental Fig. S3*B* and data not shown), we performed knockdown experiments using the same assay cell line, NF-κB-MinP-Luc-A3. The efficiency and specificity of each of the designed shRNAs were confirmed by semi-quantitative RT-PCR or immunoblotting using 293FT cells (supplemental Fig. S3, *B* and

C). The NF-κB-MinP-Luc-A3 cell line was transfected with a vector that expresses shRNA targeting each candidate protein and the catalytic subunits of the SWI/SNF complex as well as a control shRNA vector (CV-3). At 42 h after transfection, cultures were treated with or without TNF-α for an additional 6 h.

Upon TNF-α stimulation, Luc activity increased by 1400-fold when the cells were transfected with CV-3. The knockdown of Brm and BRG1, the alternative catalytic subunits of the SWI/SNF complex, caused a significant reduction in transactivation by 82 and 66%, respectively (Fig. 1*D, lanes 11* and *12*), indicating that NF-κB-MinP in the reporter cell line requires the SWI/SNF complex to be activated through the NF-κB canonical pathway. The depletion of DPF2 (Fig. 1*D, lanes 4* and *5*) and PHF-10 (Fig. 1*D, lanes 9* and *10*) lowered the ability of TNF-α to activate this promoter by 60 and 40% respectively, and the knockdown of DPF1 (Fig. 1*D, lanes 2* and *3*) marginally but clearly reduced the Luc promoter activity. These results are consistent with the notion deriving from the results of the overexpression experiments (Fig. 1*C*) that DPF1, DPF2, and PHF10 contribute to transactivation via the endogenous RelA/p50 dimer and the difference among the effects of each knockdown might be somehow reflecting their endogenous levels. Interestingly, the simultaneous depletion of DPF3a and DPF3b by a single shRNA, whose targeting site is within the shared region for these proteins, was shown to reduce TNF-α-dependent activation by 84% (Fig. 1*D, lane 6*). Furthermore, a single knockdown of either DPF3a or DPF3b also caused a comparative reduction in promoter activation (Fig. 1*D, lanes 7* and *8*). These results suggest that in these cells, among the tested candidates, either DPF3a or DPF3b have the most crucial role in the canonical NF-κB pathway, which cannot be efficiently compensated for by the other candidate proteins. The overall results shown in Fig. 1*D* were almost identically obtained using another 293FT clone K5 (supplemental Fig. S5). Taken together, these data support the idea that in 293FT cells DPF3a and DPF3b are the most critical factors required for RelA/p50 to activate this NF-κB-containing promoters in an SWI/SNF-dependent manner, and we therefore decided to further concentrate our analysis on DPF3a and DPF3b.

Both DPF3a and DPF3b Directly Bind to RelA and p50 as Well as Several Subunits of the SWI/SNF Complex in Vitro—Because DPF3a and DPF3b were found to be required for SWI/SNF complex-dependent RelA/p50 transactivation, we next evaluated the proteins with which DPF3a and DPF3b can associate *in vitro*. We first performed glutathione *S*-transferase pulldown assays using purified GST alone, GST-DPF3a, and -DPF3b and several subunits of the SWI/SNF complex translated *in vitro* in the presence of [^{35}S]methionine (supplemental Fig. S6). Both DPF3a and DPF3b directly bound to Brm, BRG1, Ini1, and BAF60a but not to β-actin, which are similar binding properties to those of DPF2 that we have previously reported (19).

We next performed a similar assay using *in vitro* translated RelA and p50 and GST-fused DPF3a and DPF3b as well as DPF2. As shown in Fig. 2*A*, either RelA or p50 alone as well as in combination with both proteins synthesized in the same translating mixture were found to directly associate with DPF3a and DPF3b. We also found that RelA or p50 alone also binds to DPF2 to a lesser extent. These binding properties of DPF2 are fully consistent with our previous report (19). In the current experiments, these two GST proteins were tagged with His_6 at their C termini to enable higher purification and the performance of a more sensitive binding assay (supplemental Fig. S7). We performed further GST pulldown assays using the same purified GST proteins and 293FT whole cell extracts obtained from cells stimulated with or without TNF-α as the input proteins. The extracts were treated with benzonase endonuclease to avoid detecting interactions mediated through DNA or RNA fragments. The pulled down cellular proteins were analyzed by immunoblotting, and as shown in Fig. 2*B*, both DPF3a and DPF3b were found to associate with endogenous RelA and BRG1. Importantly, the binding affinities for DPF3a and DPF3b in these cases were not significantly increased by TNF-α stimulation. It should be pointed out here that in the total protein preparations subcellular localization of natural NF-κB is disrupted. These results therefore suggest that the binding potential of RelA to DPF3a and DPF3b is not significantly enhanced by post-translational modifications of RelA triggered by TNF-α stimulation (25–28). Taken together, our findings indicate that both DPF3a and DPF3b have the potential to directly associate with RelA/p50 and the SWI/SNF complex and further that the binding potential is not enhanced by post-translational modifications of NF-κB or the SWI/SNF complex triggered by TNF-α.

DPF3 Interacts with the SWI/SNF Complexes and RelA/p50 in the Nucleus—We prepared 293FT cells stably expressing either FLAG-tagged DPF3a or DPF3b through the introduction of retrovirus vectors (293FT-FLAG-DPF3a and 293FT-FLAG-DPF3b) and isolated nuclear fractions from each cell type with or without TNF-α treatment. We then performed a co-immunoprecipitation assay using α-FLAG antibodies (Fig. 2*C*). The subunits of the SWI/SNF complex, Brm, BRG1, and BAF155, were found to be co-immunoprecipitated with either DPF3a or DPF3b, independently of TNF-α stimulation. In the immunoprecipitates with FLAG-DPF3b, both RelA and p50 were detected specifically in TNF-α-stimulated cells, indicating that DPF3b efficiently associates with both RelA and p50, which are recruited to the nucleus. In the immunoprecipitates with FLAG-DPF3a from TNF-α-stimulated cells, p50 was detected, whereas only marginal levels of RelA were detectable, suggesting that DPF3a binds RelA/p50 at a lower affinity than DPF3b in the nucleus. Our observations therefore suggest that the association between DPF3a/b and RelA/p50 occurs following RelA/p50 translocation to the nucleus where DPF3a or -3b consistently interacts with the SWI/SNF complex. When similar analyses were performed on the other candidate proteins, DPF1 and DPF2 showed similar binding properties to DPF3a and -3b for the associations with the SWI/SNF complex and RelA/p50 (supplemental Fig. S8).

To further analyze the DPF3 interaction with the RelA/p50 and SWI/SNF complex, we prepared whole cell extracts from 293FT-FLAG-DPF3a and 293FT-FLAG-DPF3b with or without TNF-α treatment (Fig. 2*D*). Each cellular extract was again treated with benzonase endonuclease and then subjected to a co-immunoprecipitation assay using α-FLAG antibodies. Brm, BRG1, BAF155, and BAF60a were all successfully co-immunoprecipitated from the total cellular lysates of both 293FT-

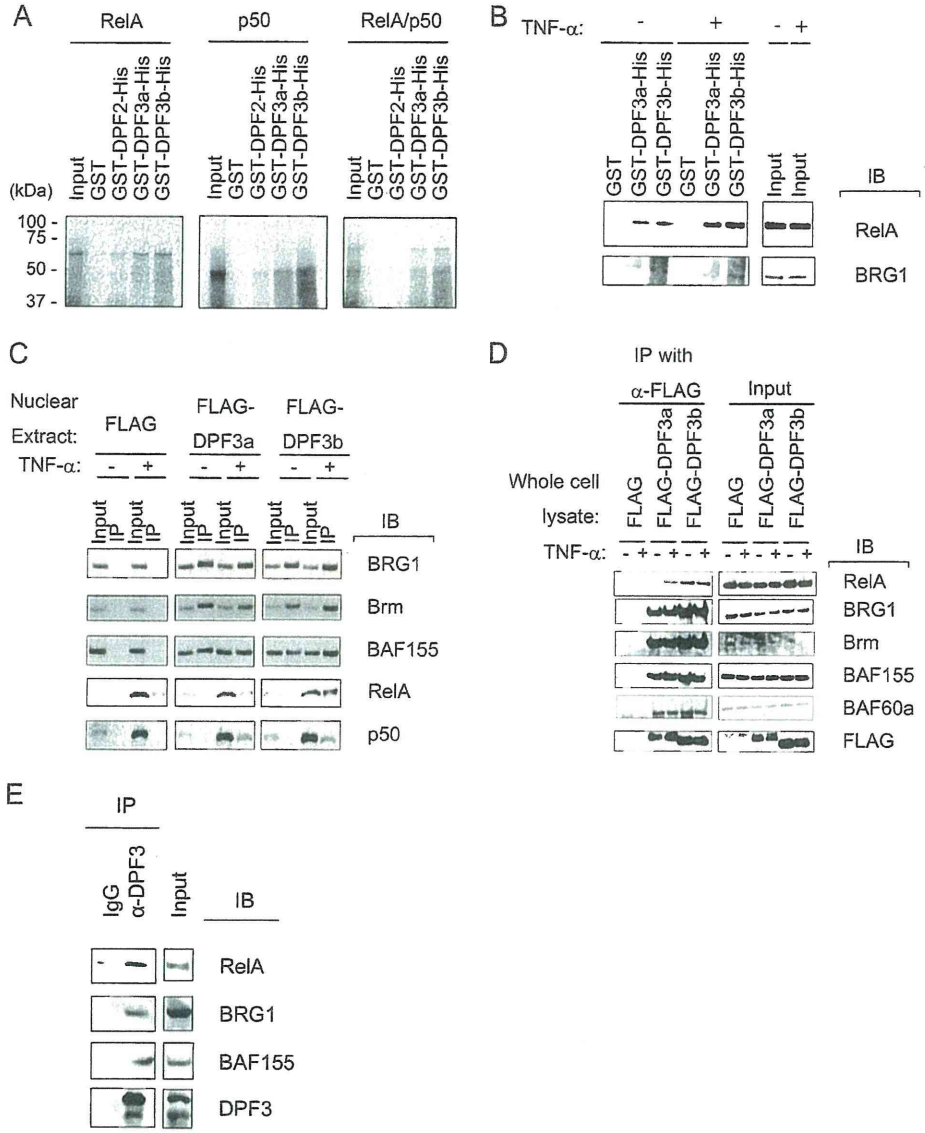

FIGURE 2. **DPF3a and -3b associate with both RelA/p50 and the SWI/SNF complex.** *A*, [^{35}S]methionine-labeled RelA and p50 were translated using a wheat germ extract system *in vitro* and incubated with GST alone and GST-His-tagged DPF2, DPF3a, or DPF3b. These interactions were analyzed by SDS-PAGE followed by autoradiography. *B*, 293FT cells were stimulated with or without 10 ng/ml TNF-α for 10 min, and whole cell lysates were then obtained and subjected to benzonase endonuclease treatment. The lysate was incubated with GST alone, GST-His-tagged DPF2, DPF3a, or DPF3b, and pulled down materials were analyzed by immunoblotting. *C*, 293FT cells were stimulated with or without 10 ng/ml TNF-α for 10 min, and whole cell lysates were obtained and treated with endonuclease. Immunoprecipitation (*IP*) assays were performed using α-FLAG antibodies, and precipitated materials were eluted with free FLAG peptide and analyzed by immunoblotting (*IB*). *D*, 293FT cells stably expressing FLAG, FLAG-DPF3a, or FLAG-DPF3b were stimulated with or without 10 ng/ml TNF-α for 60 min. Nuclear extracts were then prepared and subjected to immunoprecipitation assays with α-FLAG antibodies followed by immunoblotting. *E*, 293FT cells were treated with 10 ng/ml TNF-α for 20 min, and whole cell lysate was obtained and treated with endonuclease. Immunoprecipitation assays were performed using α-DPF3 antibody, and precipitated materials were analyzed by immunoblotting.

FLAG-DPF3a and -DPF3b independently of TNF-α. RelA was found to be co-immunoprecipitated with DPF3b and to a lesser extent with DPF3a. DPF3a and DPF3b would associate with RelA after the preparation of the whole cell extracts from unstimulated cells, where the natural NF-κB subcellular localizations are disrupted. These data again support that the RelA binding potential to DPF3a or DPF3b was not significantly affected by TNF-α treatment, consistent with the results shown in Fig. 2*B*.

To finally show our observations that DPF3a/b associates with RelA/p50 or the SWI/SNF complex is valid even in non-manipulated cells, we treated 293FT cells with TNF-α for 20 min and immunoprecipitated endogenous DPF3a and DPF3b with antibody against DPF3, which does not discriminate between DPF3a and DPF3b. The immunoprecipitates were analyzed, and endogenous DPF3a/b was shown to associate with RelA, BRG1, and BAF155, just like exogenously introduced DPF3 proteins (Fig. 2*E*).

Kinetics of RelA Recruitment upon TNF-α Stimulation Correlate with Those of Primary Transcript Production from Both Artificial and Natural Promoters—To understand molecular mechanisms involved in transcriptional activation after TNF-α stimulation, we next analyzed the kinetics of RelA recruitment and transactivation. Following cellular exposure to TNF-α, it

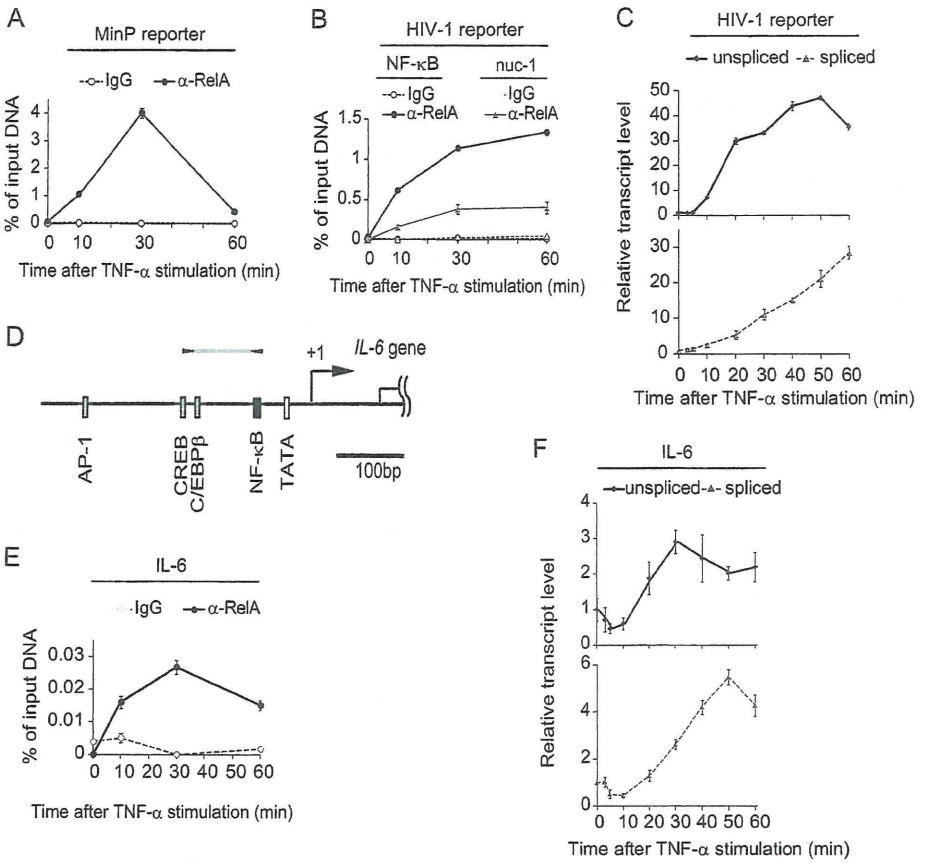

FIGURE 3. **Kinetics of RelA recruitment upon TNF-α stimulation correlate with the primary transcript production levels from both artificial and native promoters.** *A, B,* and *E,* kinetics of RelA recruitment to NF-κB-MinP (*A*), HIV-1 LTR (*B*), and the endogenous IL-6 promoter (*E*) upon TNF-α stimulation. Cells were treated with 10 ng/ml TNF-α for the indicated times and were harvested and precipitated by antibodies against RelA or with a normal rabbit IgG control. The immunoprecipitated DNA was quantified by real time PCR and normalized relative to the input. *C* and *F,* real time RT-PCR analysis of transcripts of HIV-1 LTR (*C*) and the endogenous IL-6 promoter (*F*). Cells were treated with 10 ng/ml TNF-α for the indicated times, and mRNA was prepared. Spliced and unspliced mRNAs were quantified, and these levels were normalized to individual untreated samples. *D,* schematic representation of the *IL-6* promoter region. The binding site for NF-κB and other transcription factors and the TATA box are highlighted by *black, gray,* and *white bars,* respectively. Transcriptional start sites are designated as +1. Positions detected by real time PCR are indicated by *black arrows* and a *gray bar.*

was previously reported at a single cell resolution that RelA oscillates dynamically between the nucleus and the cytoplasm and that this oscillation cycle is about 1 h (29). To analyze the primary effects of TNF-α stimulation on RelA/p50 transactivation, we performed ChIP analysis of the promoters of the reporter genes after stimulation within 1 h. In NF-κB-MinP-Luc-A3 cells, the results showed that the stimulation-dependent recruitment of RelA achieved a peak at 30 min post-treatment and drastically reduced to marginal levels within 60 min (Fig. 3*A*). Next, by using 293FT cells harboring an HIV-1-based reporter provirus (293FT-LTR-Luc-5; Fig. 1*B*) instead, we performed the same set of analyses (Fig. 3*B*). Interestingly, RelA recruitment to the NF-κB-responsive elements within the HIV-1 LTR kept increasing during the first 60 min after TNF-α stimulation with small leakage of the signal detected in the nucleosome 1 (nuc-1) region. Considering that the nucleotide sequences of the NF-κB elements are identical in both of these promoters, it is noteworthy that distinct kinetics of RelA recruitment were observed, *i.e.* the wild type HIV-1 LTR retains RelA longer.

We next analyzed whether there was any association between the recruitment levels of RelA and the transactivation kinetics of these promoters. By quantifying the HIV-1 LTR transcript levels at the indicated time points by real time RT-PCR, we found that the kinetics of the *de novo* synthesized primary unspliced mRNAs were very similar to those of RelA recruitment, whereas those of the mature spliced mRNAs kept increasing (Fig. 3*C*). Because the primary transcript of NF-κB-MinP does not contain introns, it cannot be distinguished from the mature mRNA. Interestingly, using a promoter of an endogenous TNF-α-inducible gene, IL-6 (Fig. 3*D*), which requires the SWI/SNF complex for activation (14), we observed a good correlation in kinetics between RelA recruitment and primary transcript synthesis after TNF-α stimulation (Fig. 3, *E* and *F*, and the induction kinetics is more prompt than those observed for HIV-1 LTR in the same cells (Fig. 3*B*). In addition, the kinetics of the recruitment of RelA to the *IL-6* promoter are similar to those of NF-κB-MinP, achieving a peak at 30 min after stimulation and decreasing at 60 min. Our present observations thus suggest that HIV-1 LTR retains RelA longer against the oscillation cycle of RelA between the nucleus and the cytoplasm. HIV-1 LTR contains many binding sites for other transcription factors, some of which would associate with RelA (30–32). This might cause differences in the kinetics of the

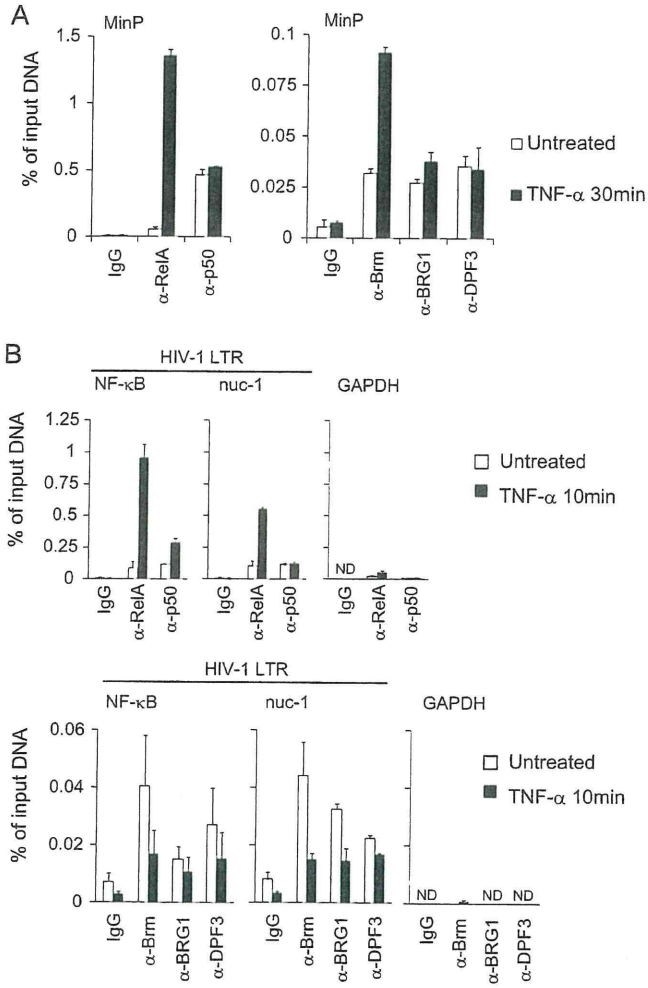

FIGURE 4. **Chromatin dynamics and recruitment of DPF3 and RelA/p50 to SWI/SNF-dependent promoters upon TNF-α treatment.** ChIP analysis was performed, and the data were quantified as described in Fig. 3. *A*, ChIP analysis of RelA, p50, Brm, BRG1, and DPF3 levels at the NF-κB-MinP upon TNF-α stimulation. *B*, recruitment of RelA, p50, Brm, BRG1, BAF60a, Ini1, and DPF3 to the regions within the HIV-1 LTR and GAPDH promoter after TNF-α treatment. Results presented here are the average of at least two independent experiments. *ND*, not detectable.

artificial MinP, which is simply under the control of NF-κB. However, the endogenous *IL-6* promoter is also regulated by other transcription regulators but showed no retention of RelA. This observation might be reflecting that, unlike HIV-1 LTR, this gene is expected to be strictly down-regulated after the stimulation for proper inflammatory response.

Chromatin Dynamics around the NF-κB-binding Sites in Both Artificial and Native Promoters after TNF-α Treatment—We next analyzed the dynamics of endogenous DPF3 and the SWI/SNF complex as well as RelA/p50 for both NF-κB-MinP and HIV-1 LTR in response to TNF-α stimuli. Consistent with Fig. 3*A*, this stimulation caused a dynamic recruitment of RelA to NF-κB-MinP at 30 min (*left panel* of Fig. 4*A*). Similar amounts of NF-κB p50 subunit were detected both before and after TNF-α stimulation, which we think is consistent with previous observations that low levels of the p50 subunit are present on specific NF-κB-responsive promoters in the nucleus of unstimulated cells as the p50 homodimer, whereas the majority of this subunit is retained in the cytoplasm as RelA/p50 (33–35). The p50 homodimer itself does not contain transactivation domains, but it associates with promoter regions of some NF-κB-dependent genes, including integrated HIV-1 LTR in the unstimulated conditions (36). However, Brm, BRG1, and DPF3 were all detected at the promoter even before stimulation, and their recruitment levels were not significantly changed upon exposure to TNF-α, apart from Brm, which showed elevated levels at the promoter (*right panel* of Fig. 4*A*). In the case of 293FT-LTR-Luc-5 cells, RelA was recruited to NF-κB elements in the HIV-1 LTR within 10 min of stimulation, whereas the NF-κB p50 subunit was found to be constitutively present in the LTR (*upper panel* of Fig. 4*B*). Brm, BRG1, and DPF3 were also detected at the promoter prior to TNF-α treatment, and their recruitment levels were reduced by about 50% after stimulation, suggesting that upon transcriptional activation, the SWI/SNF complex partially releases from the promoter with DPF3 (*lower panel* of Fig. 4*B*). Because other subunits of the complex such as BAF60a and Ini1 behaved in a similar manner to Brm or BRG1 (supplemental Fig. S9), we speculate that the changes in the levels of the catalytic subunits associated with the HIV-LTR promoter were as part of the SWI/SNF complex.

Whereas the two promoters under analysis showed different RelA recruitment kinetics, they were found to share two important features from our observations. First, endogenous DPF3 together with the SWI/SNF complex is bound to the promoters prior to TNF-α stimulation. Second, upon stimulation, RelA/p50, which can directly interact with DPF3 (Fig. 2*A*), was found to be rapidly recruited to the promoters, and this recruitment was shown to be associated with transcriptional activation, as judged by the primary transcript levels.

Finally, we analyzed the endogenous *IL-6* promoter to check whether DPF3 links the SWI/SNF complex and RelA/p50 forming a larger complex. ChIP analysis showed that both RelA and DPF3a/b were recruited to the promoter in a TNF-α-dependent and -independent manner, respectively (Fig. 5*A*). To perform sequential ChIP analysis, the immunoprecipitates with α-RelA antibody were re-immunoprecipitated with antibodies specific for DPF3a/b and Brm as well as the α-RelA antibody (positive control) and normal rabbit IgG (negative control), respectively (Fig. 5*B*). The second round of immunoprecipitates using α-DPF3 and Brm antibodies indicated that DPF3 and the SWI/SNF complex co-associate with RelA on the *IL-6* promoter after the RelA/p50 heterodimer is recruited upon TNF-α stimulation. In conclusion, all these results support that DPF3a and -3b link the SWI/SNF complex to NF-κB to transactivate the target promoters that require chromatin remodeling for the transcriptional initiation.

DISCUSSION

By extending our previous observation that DPF2 links RelB/p52 and the SWI/SNF complex for NF-κB transactivation via its noncanonical pathway, we have here shown that each of the five proteins, DPF1, DPF2, DPF3a, DPF3b, and PHF10, can equally function as an efficient co-activator of the RelA/p50 dimer at the most downstream part of the NF-κB canonical pathway, when they are exogenously expressed at high levels

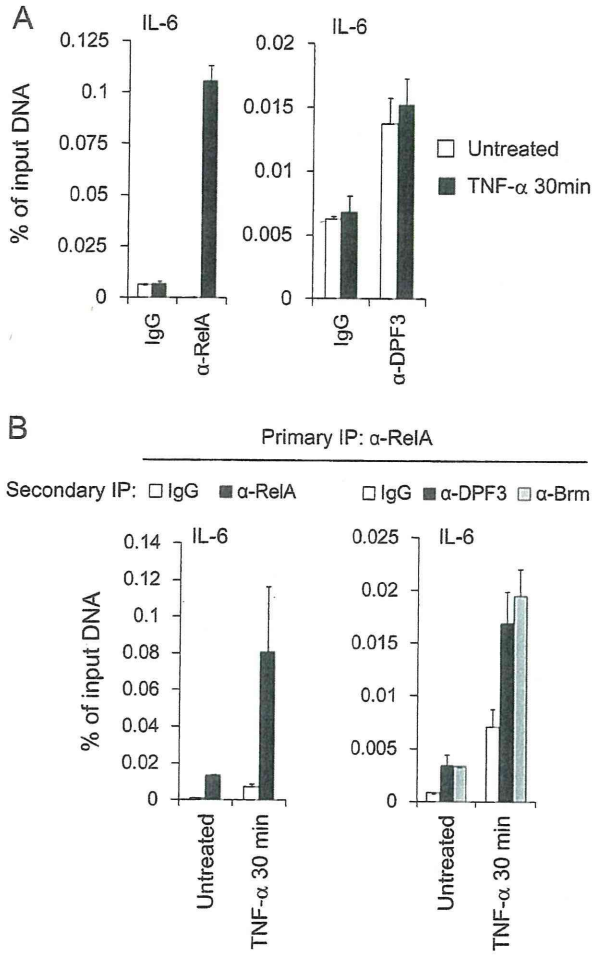

FIGURE 5. **ChIP and re-ChIP assays at the endogenous *IL-6* promoter.** *A*, ChIP analysis of RelA and DPF3 occupancy levels at the *IL-6* promoter. 293FT cells were treated with or without 10 ng/ml TNF-α for 30 min and harvested for precipitation by antibodies against RelA and DPF3. *B*, primary immunoprecipitated materials concentrated with α-RelA antibody were followed by secondary rounds of immunoprecipitations with indicated antibodies. Immunoprecipitated materials were quantified by real time PCR.

(Fig. 1*C*). Under these conditions, each of these proteins activated the other two representative NF-κB dimers, RelB/p52 and c-Rel/p50, with similar efficiencies. When these five proteins were expressed by retrovirus vectors, they are constitutively binding to the SWI/SNF complex in the nucleus and begin to associate with RelA/p50 upon TNF-α treatment (Fig. 2*C* and supplemental Fig. S8). From these results, we think each of these proteins would function as a co-activator of NF-κB in certain tissues. DPF1 was reported to be neurospecific and play an important role in developing neurons (20, 24). DPF2, which is ubiquitously expressed, is known to be involved in the processes of apoptosis in mouse myeloid cells following interleukin 3 (IL-3) deprivation (37). In normal cells, DPF3a/b was reported to be expressed specifically in cardiac and skeletal muscle and was critical for heart and muscle development (23). Because NF-κB plays important roles in programmed cell death and development, these d4 proteins might be involved in these physiological phenomena through activating some specific NF-κB dimers. Because DPF1, DPF2, DPF3b and PHF10 contain double PHD fingers, which are not possessed by any of the core subunits of the SWI/SNF complex, they are likely to play some roles in selecting specific species of modified histones in the nucleosomes at target promoter regions.

In 293FT cells, which express only low levels of endogenous mRNAs for the five candidate protein co-activators, the knockdown of either DPF3a or DPF3b suppressed TNF-α-induced NF-κB transactivation to marginal levels, suggesting that both proteins are essential for the NF-κB canonical pathway (Fig. 1*D*). Currently, we cannot fully explain this observation, but there could be several possibilities. One possibility would be that the SWI/SNF complex needs to bind both DPF3a and DPF3b to perform its full function for NF-κB transactivation. We would, however, prefer another possibility as follows. DPF3a and DPF3b share roles in NF-κB transactivation probably through their common N-terminal regions. The endogenous cellular amounts of both proteins in 293FT cells are so low (supplemental Fig. S3) that depletion of either would drastically reduce their recruitment frequency to the promoter of the reporter, where a single molecule of either DPF3a or DPF3b is sufficient for the SWI/SNF complex to perform full transactivation. Because DPF3a lacks functional PHD fingers, however, it is also possible that they would show distinct promoter preferences in some cases, as has been shown previously by ChIP analysis of exogenously expressed DPF3a and DPF3b (23).

We have previously shown that a representative target gene of the NF-κB canonical pathway, *IL-8*, is induced in HeLa cells by TNF-α and that this induction is not affected by the knockdown of DPF2. We suggested from this that DPF2 does not significantly contribute to the NF-κB canonical pathway, at least in this cell system. Because the endogenous *IL-8* gene was found not to be affected by the knockdown of either catalytic subunit of the SWI/SNF complex (19), we believe that this promoter is induced independently of SWI/SNF. In immune cells, some NF-κB target promoters have also been reported not to require chromatin remodeling for their transcriptional initiation upon LPS stimulation, because they already possess an open chromosome structure (38).

Importantly, with respect to our current investigations, the results of ChIP analysis using antiserum that we prepared indicated that the endogenous DPF3 proteins (this antiserum does not discriminate between DPF3a and DPF3b) as well as the SWI/SNF complex are recruited continuously to the promoters we examined, NF-κB-MinP and wild type HIV-1 LTR. Considering that both DPF3a and DPF3b directly bind to p50 *in vitro*, we speculate that DPF3a/3b together with the SWI/SNF complex locate near the NF-κB-binding sites through the binding of the p50 homodimer under unstimulated conditions but through active RelA/p50 upon stimulation. This dimer substitution would then trigger SWI/SNF-dependent transactivation. Hence, the SWI/SNF complex would be present at these target promoters to facilitate the ready recruitment of RelA/p50 for the prompt remodeling of the surrounding chromatin structures. Considering our observations that transcriptional enhancement of HIV-1 LTR occurs just after the SWI/SNF complex and RelA/p50 get together on the promoter (Figs. 3, *B* and *C*, and 4*B*), DPF3a/3b is significant for this activation as a linker protein.

Acknowledgments—We thank S. Kawaura and A. Kato for their assistance in preparing this manuscript. We thank Dr. H. Nakano and Dr. H. Watanabe for critical reading of this manuscript.

REFERENCES

1. Beinke, S., and Ley, S. C. (2004) Functions of NF-κB1 and NF-κB2 in immune cell biology. *Biochem. J.* **382,** 393–409
2. Santoro, M. G., Rossi, A., and Amici, C. (2003) NF-κB and virus infection. Who controls whom. *EMBO J.* **22,** 2552–2560
3. Vallabhapurapu, S., and Karin, M. (2009) Regulation and function of NF-κB transcription factors in the immune system. *Annu. Rev. Immunol.* **27,** 693–733
4. Ben-Neriah, Y., and Karin, M. (2011) Inflammation meets cancer, with NF-κB as the matchmaker. *Nat. Immunol.* **12,** 715–723
5. Gilmore, T. D. (2006) Introduction to NF-kappaB: players, pathways, perspectives. *Oncogene* **25,** 6680–6684
6. Ghosh, S., May, M. J., and Kopp, E. B. (1998) NF-κB and Rel proteins. Evolutionarily conserved mediators of immune responses. *Annu. Rev. Immunol.* **16,** 225–260
7. Pomerantz, J. L., and Baltimore, D. (2002) Two pathways to NF-κB. *Mol. Cell* **10,** 693–695
8. Muchardt, C., and Yaniv, M. (1999) ATP-dependent chromatin remodeling. SWI/SNF and Co. are on the job. *J. Mol. Biol.* **293,** 187–198
9. Wilson, B. G., and Roberts, C. W. (2011) SWI/SNF nucleosome remodelers and cancer. *Nat. Rev. Cancer* **11,** 481–492
10. Kwon, H., Imbalzano, A. N., Khavari, P. A., Kingston, R. E., and Green, M. R. (1994) Nucleosome disruption and enhancement of activator binding by a human SWI/SNF complex. *Nature* **370,** 477–481
11. Cheng, S. W., Davies, K. P., Yung, E., Beltran, R. J., Yu, J., and Kalpana, G. V. (1999) c-MYC interacts with INI1/hSNF5 and requires the SWI/SNF complex for transactivation function. *Nat. Genet.* **22,** 102–105
12. Kowenz-Leutz, E., and Leutz, A. (1999) A C/EBPβ isoform recruits the SWI/SNF complex to activate myeloid genes. *Mol. Cell* **4,** 735–743
13. Ito, T., Yamauchi, M., Nishina, M., Yamamichi, N., Mizutani, T., Ui, M., Murakami, M., and Iba, H. (2001) Identification of SWI.SNF complex subunit BAF60a as a determinant of the transactivation potential of Fos/Jun dimers. *J. Biol. Chem.* **276,** 2852–2857
14. Watanabe, H., Mizutani, T., Haraguchi, T., Yamamichi, N., Minoguchi, S., Yamamichi-Nishina, M., Mori, N., Kameda, T., Sugiyama, T., and Iba, H. (2006) SWI/SNF complex is essential for NRSF-mediated suppression of neuronal genes in human nonsmall cell lung carcinoma cell lines. *Oncogene* **25,** 470–479
15. Yamamichi, N., Inada, K., Furukawa, C., Sakurai, K., Tando, T., Ishizaka, A., Haraguchi, T., Mizutani, T., Fujishiro, M., Shimomura, R., Oka, M., Ichinose, M., Tsutsumi, Y., Omata, M., and Iba, H. (2009) Cdx2 and the Brm-type SWI/SNF complex cooperatively regulate villin expression in gastrointestinal cells. *Exp. Cell Res.* **315,** 1779–1789
16. Iba, H., Mizutani, T., and Ito, T. (2003) SWI/SNF chromatin remodeling complex and retroviral gene silencing. *Rev. Med. Virol.* **13,** 99–110
17. Mizutani, T., Ito, T., Nishina, M., Yamamichi, N., Watanabe, A., and Iba, H. (2002) Maintenance of integrated proviral gene expression requires Brm, a catalytic subunit of SWI/SNF complex. *J. Biol. Chem.* **277,** 15859–15864
18. Mizutani, T., Ishizaka, A., Tomizawa, M., Okazaki, T., Yamamichi, N., Kawana-Tachikawa, A., Iwamoto, A., and Iba, H. (2009) Loss of the Brm-type SWI/SNF chromatin remodeling complex is a strong barrier to the Tat-independent transcriptional elongation of human immunodeficiency virus type 1 transcripts. *J. Virol.* **83,** 11569–11580
19. Tando, T., Ishizaka, A., Watanabe, H., Ito, T., Iida, S., Haraguchi, T., Mizutani, T., Izumi, T., Isobe, T., Akiyama, T., Inoue, J., and Iba, H. (2010) Requiem protein links RelB/p52 and the Brm-type SWI/SNF complex in a noncanonical NF-κB pathway. *J. Biol. Chem.* **285,** 21951–21960
20. Buchman, V. L., Ninkina, N. N., Bogdanov, Y. D., Bortvin, A. L., Akopian, H. N., Kiselev, S. L., Krylova OYu., Anokhin, K. V., and Georgiev, G. P. (1992) Differential splicing creates a diversity of transcripts from a neuro-specific developmentally regulated gene encoding a protein with new zinc finger motifs. *Nucleic Acids Res.* **20,** 5579–5585
21. Chestkov, A. V., Baka, I. D., Kost, M. V., Georgiev, G. P., and Buchman, V. L. (1996) The d4 gene family in the human genome. *Genomics* **36,** 174–177
22. Ninkina, N. N., Mertsalov, I. B., Kulikova, D. A., Alimova-Kost, M. V., Simonova, O. B., Korochkin, L. I., Kiselev, S. L., and Buchman, V. L. (2001) Cerd4, third member of the d4 gene family. Expression and organization of genomic locus. *Mamm. Genome* **12,** 862–866
23. Lange, M., Kaynak, B., Forster, U. B., Tönjes, M., Fischer, J. J., Grimm, C., Schlesinger, J., Just, S., Dunkel, I., Krueger, T., Mebus, S., Lehrach, H., Lurz, R., Gobom, J., Rottbauer, W., Abdelilah-Seyfried, S., and Sperling, S. (2008) Regulation of muscle development by DPF3, a novel histone acetylation and methylation reader of the BAF chromatin remodeling complex. *Genes Dev.* **22,** 2370–2384
24. Lessard, J., Wu, J. I., Ranish, J. A., Wan, M., Winslow, M. M., Staahl, B. T., Wu, H., Aebersold, R., Graef, I. A., and Crabtree, G. R. (2007) An essential switch in subunit composition of a chromatin remodeling complex during neural development. *Neuron* **55,** 201–215
25. Chaturvedi, M. M., Sung, B., Yadav, V. R., Kannappan, R., and Aggarwal, B. B. (2011) NF-κB addiction and its role in cancer. "One size does not fit all." *Oncogene* **30,** 1615–1630
26. Perkins, N. D. (2006) Post-translational modifications regulating the activity and function of the nuclear factor κB pathway. *Oncogene* **25,** 6717–6730
27. Schmitz, M. L., Mattioli, I., Buss, H., and Kracht, M. (2004) NF-κB. A multifaceted transcription factor regulated at several levels. *ChemBioChem* **5,** 1348–1358
28. Viatour, P., Merville, M. P., Bours, V., and Chariot, A. (2005) Phosphorylation of NF-κB and IκB proteins. Implications in cancer and inflammation. *Trends Biochem. Sci.* **30,** 43–52
29. Nelson, D. E., Ihekwaba, A. E., Elliott, M., Johnson, J. R., Gibney, C. A., Foreman, B. E., Nelson, G., See, V., Horton, C. A., Spiller, D. G., Edwards, S. W., McDowell, H. P., Unitt, J. F., Sullivan, E., Grimley, R., Benson, N., Broomhead, D., Kell, D. B., and White, M. R. (2004) Oscillations in NF-κB signaling control the dynamics of gene expression. *Science* **306,** 704–708
30. Stevens, M., De Clercq, E., and Balzarini, J. (2006) The regulation of HIV-1 transcription. Molecular targets for chemotherapeutic intervention. *Med. Res. Rev.* **26,** 595–625
31. Rohr, O., Marban, C., Aunis, D., and Schaeffer, E. (2003) Regulation of HIV-1 gene transcription. From lymphocytes to microglial cells. *J. Leukocyte Biol.* **74,** 736–749
32. Pereira, L. A., Bentley, K., Peeters, A., Churchill, M. J., and Deacon, N. J. (2000) A compilation of cellular transcription factor interactions with the HIV-1 LTR promoter. *Nucleic Acids Res.* **28,** 663–668
33. Satou, R., Miyata, K., Katsurada, A., Navar, L. G., and Kobori, H. (2010) Tumor necrosis factor-α suppresses angiotensinogen expression through formation of a p50/p50 homodimer in human renal proximal tubular cells. *Am. J. Physiol. Cell Physiol.* **299,** C750–C759
34. Wu, Z. Z., Chow, K. P., Kuo, T. C., Chang, Y. S., and Chao, C. C. (2011) Latent membrane protein 1 of Epstein-Barr virus sensitizes cancer cells to cisplatin by enhancing NF-κB p50 homodimer formation and down-regulating NAPA expression. *Biochem. Pharmacol.* **82,** 1860–1872
35. Zhong, H., May, M. J., Jimi, E., and Ghosh, S. (2002) The phosphorylation status of nuclear NF-κB determines its association with CBP/p300 or HDAC-1. *Mol. Cell* **9,** 625–636
36. Williams, S. A., Chen, L. F., Kwon, H., Ruiz-Jarabo, C. M., Verdin, E., and Greene, W. C. (2006) NF-κB p50 promotes HIV latency through HDAC recruitment and repression of transcriptional initiation. *EMBO J.* **25,** 139–149
37. Gabig, T. G., Mantel, P. L., Rosli, R., and Crean, C. D. (1994) Requiem. A novel zinc finger gene essential for apoptosis in myeloid cells. *J. Biol. Chem.* **269,** 29515–29519
38. Ramirez-Carrozzi, V. R., Braas, D., Bhatt, D. M., Cheng, C. S., Hong, C., Doty, K. R., Black, J. C., Hoffmann, A., Carey, M., and Smale, S. T. (2009) A unifying model for the selective regulation of inducible transcription by CpG islands and nucleosome remodeling. *Cell* **138,** 114–128

Translational inhibition by deadenylation-independent mechanisms is central to microRNA-mediated silencing in zebrafish

Yuichiro Mishima[a,1], Akira Fukao[b,2], Tomoyoshi Kishimoto[a,2], Hiroshi Sakamoto[a], Toshinobu Fujiwara[b], and Kunio Inoue[a,1]

[a]Department of Biology, Graduate School of Science, Kobe University, 1-1 Rokkodaicho Nadaku, Kobe, Hyogo 657-8501, Japan; and [b]Institute of Microbial Chemistry, 3-14-23 Kamiosaki, Shinagawa-ku, Tokyo 141-0021, Japan

Edited by Joan A. Steitz, Howard Hughes Medical Institute, New Haven, CT, and approved December 5, 2011 (received for review August 15, 2011)

MicroRNA (miRNA) is a class of small noncoding RNA approximately 22 nt in length. Animal miRNA silences complementary mRNAs via translational inhibition, deadenylation, and mRNA degradation. However, the underlying molecular mechanisms remain unclear. A key question is whether these three outputs are independently induced by miRNA through distinct mechanisms or sequentially induced within a single molecular pathway. Here, we successfully dissected these intricate outputs of miRNA-mediated repression using zebrafish embryos as a model system. Our results indicate that translational inhibition and deadenylation are independent outputs mediated by distinct domains of TNRC6A, which is an effector protein in the miRNA pathway. Translational inhibition by TNRC6A is divided into two mechanisms: PAM2 motif-mediated interference of poly(A)-binding protein (PABP), and inhibition of 5′ cap- and poly(A) tail-independent step(s) by a previously undescribed P-GL motif. Consistent with these observations, we show that, in zebrafish embryos, miRNA inhibits translation of the target mRNA in a deadenylation- and PABP-independent manner at early time points. These results indicate that miRNA exerts multiple posttranscriptional outputs via physically and functionally independent mechanisms and that direct translational inhibition is central to miRNA-mediated repression.

MicroRNA (miRNA) is a class of small noncoding RNA approximately 22 nt in length. Previous studies have shown that miRNA plays a wide variety of regulatory roles in animals and plants (1). Animal miRNA silences partially complementary mRNAs (2). However, the mechanism of its action is under intense debate. Biochemical studies have shown a significant repression of miRNA target genes via translational inhibition (3). In contrast, transcriptome analyses of miRNA target genes have revealed that miRNA promotes mRNA degradation (4, 5). Genome-wide studies that analyzed mRNA stability and translation status in parallel have reached different conclusions concerning the relative contributions of these two outputs (6–8). In addition to these outputs, miRNA induces deadenylation of its target mRNA (5, 9, 10). Given that the translation status, poly(A) tail length and mRNA stability are closely linked to each other, whether these three outputs are independently induced by miRNA through distinct mechanisms or rather sequentially induced within single molecular pathway remains unknown (3, 11).

miRNA forms a complex with protein factors, called miRNA induced silencing complex (miRISC), to induce target mRNA silencing. Argonaute (Ago) protein is an integral component of miRISC and directly interacts with miRNA to support the binding of miRNAs to their target mRNAs (12). In addition to Ago, animal miRNA requires another miRISC component, TNRC6/GW182 (hereafter referred to as TNRC6), for target mRNA silencing (13). TNRC6 associates with the Ago-miRNA complex via multiple Ago-binding motifs in its N-terminal region (14, 15). In contrast, the C-terminal regions of TNRC6 have been identified as a silencing domain because this domain is sufficient to elicit posttranscriptional silencing (16, 17). Recent studies have shown that the silencing domains of TNRC6 bind to poly(A) binding protein (PABP). In the case of mammalian TNRC6, the interaction occurs mainly through direct interaction between the conserved sequence PAM2 (PABP-interacting motif 2), which is located at the anterior portion of the silencing domain, and the C-terminal MLLE domain of PABP (18–20). The TNRC6-PABP interaction accelerates deadenylation by CAF1/CCR4 in Krebs cell extract (18, 19). In human and fly cultured cells, the TNRC6-PABP interaction is required to support maximum repression by miRNA (20). These observations have led to a model proposing that, via TNRC6-PABP interactions, miRISC interferes with translation at the initiation step and/or induces mRNA deadenylation/degradation by increasing the susceptibility of the poly(A) tail to deadenylases (11, 18). However, this model does not address the hierarchy of multiple outputs induced by miRNA. In addition, the contribution of the TNRC6-PABP interaction in the miRNA pathway awaits further validation because poly(A) tail-independent repression by miRNA has been reported in several experimental systems (10, 21).

In the current study, we successfully dissected intricate outputs of miRNA-mediated repression using zebrafish embryos as a model system. Our results indicate that translational inhibition and deadenylation are independent outputs mediated by distinct domains of TNRC6A. Translational inhibition by TNRC6A is divided into two mechanisms: PAM2 motif-mediated interference of poly(A)-binding protein (PABP), and inhibition of 5′ cap- and poly(A) tail-independent step(s) by a previously undescribed P-GL motif. Consistent with these observations, we show that, in zebrafish embryos, miRNA inhibits translation of the target mRNA in a deadenylation- and PABP-independent manner at early time points.

Results

TNRC6A Induces Translational Inhibition and Deadenylation Through the Mid Domain in Zebrafish Embryos. To elucidate the mechanisms of miRNA-mediated repression, we investigated the repression activities of TNRC6 using zebrafish as an in vivo model system. As in other vertebrates, the genome of zebrafish encodes all three TNRC6 paralogues (TNRC6A, B and C) and additional TNRC6B and TNRC6C genes due to genome duplication. We focused on a unique zebrafish orthologue of TNRC6A in this study because all TNRC6 paralogues have a repressive activity in humans (17, 22). Zebrafish TNRC6A contains all of the conserved motifs/domains that were found in other TNRC6 ortholo-

Author contributions: Y.M. and K.I. designed research; Y.M., A.F., T.K., H.S., and T.F. performed research; Y.M., T.F., and K.I. analyzed data; and Y.M. and K.I. wrote the paper.

The authors declare no conflict of interest.

This article is a PNAS Direct Submission.

[1]To whom correspondence may be addressed. E-mail: yuichiro.mishima@people.kobe-u.ac.jp or kunio@kobe-u.ac.jp.

[2]A.F. and T.K. contributed equally to this work.

This article contains supporting information online at www.pnas.org/lookup/suppl/doi:10.1073/pnas.1113350109/-/DCSupplemental.

gues (13) (Fig. 1*A*). To identify the functional domain(s) in zebrafish TNRC6A that were responsible for silencing effects, we generated a series of deletion constructs and tested their effects in a λN-BoxB tethering assay in zebrafish embryos (Fig. 1 *A* and *B*). Tethering of full-length TNRC6A to Rluc-BoxB-poly(A) mRNA repressed Rluc activity to approximately 40% compared to the control construct encoding the HA-tagged N-peptide (HA-N) (Fig. 1*C*, full). As reported with other TNRC6 orthologues (16, 17), the silencing domain (SD) of zebrafish TNRC6A was sufficient to induce repression (Fig. 1*C*, SD). Furthermore, we found that the anterior half of the silencing domain (before the RRM, hereafter referred to as the Mid domain) induced repression (Fig. 1*C*, Mid). On the other hand, no significant repression was observed with TNRC6A fragments lacking the Mid domain despite detectable expression of effector proteins (Fig. 1*F*). The repression was mediated via specific binding of N-peptide fusions to BoxB sequences (Fig. S1). qRT-PCR showed that mRNA stability was not changed by tethered TNRC6A proteins during the assay (Fig. 1*D*). RNaseH-mediated poly(A) tail analysis revealed that the full-length TNRC6A, the silencing domain fragment and the Mid domain fragment induced deadenylation (Fig. 1*E*). These results reveal that the Mid domain of zebrafish TNRC6A is essential and sufficient to induce translational inhibition and deadenylation.

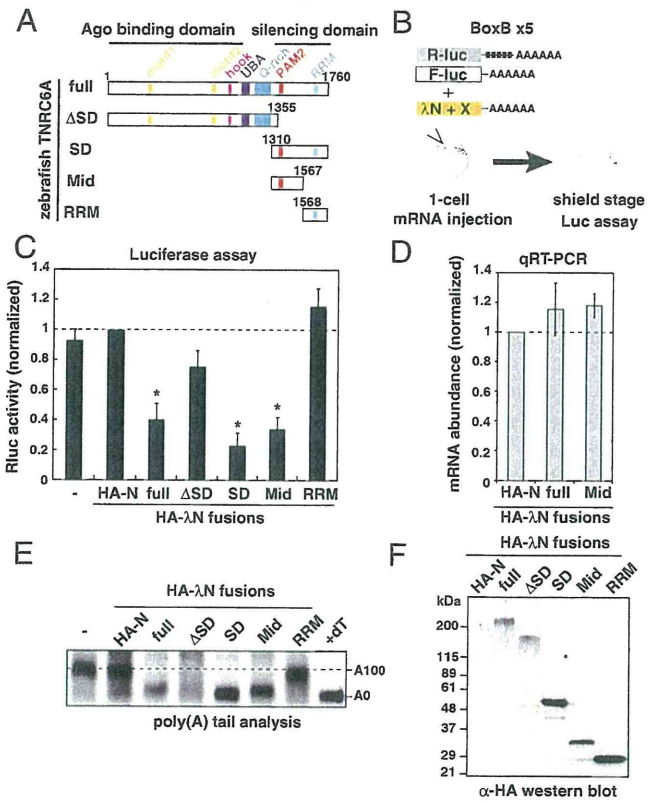

Fig. 1. The Mid domain of TNRC6A is sufficient to induce translational repression and deadenylation. (*A*) Schematic structures of zebrafish TNRC6A and its deletion mutants. (*B*) Schematic representation of the λN tethering assay in zebrafish embryos. (*C*) Results of the tethering assay with TNRC6A fragments. The bar graph shows Rluc activity that was normalized to Fluc activity. The normalized Rluc activity with the HA-λN empty construct (HA-N) was set to one. The data show averages of three independent experiments. Error bars show SD. Asterisks indicate $p < 0.01$ compared to experiments with HA-N. (*D*) The qRT-PCR analysis of reporter mRNA stability. The normalized Rluc mRNA values [normalized to those of the HA-λN empty construct (HA-N)] were set to one. The data show averages of three independent experiments. Error bars show SD. (*E*) The poly(A) tail analysis of the Rluc-BoxB-pA reporter mRNA by RNaseH digestion and Northern blot. The lane +dT shows completely deadenylated fragments, which correspond to A0. (*F*) Western blotting detecting HA-tagged effecter proteins.

A Previously Undescribed P-GL Motif in TNRC6A Contributes to Translational Inhibition in Concert with the PAM2 Motif. The PAM2 motif was conserved in the Mid domain of zebrafish TNRC6A, with critical residues for the interaction with PABP remaining invariant (Fig. 2*A*) (18–20). To determine whether the silencing activities of the Mid domain required PAM2–PABP interaction, we introduced a mutation into the PAM2 motif of the TNRC6A Mid domain (Fig. 2*A*, E1421 and F1422 to A; PAM2 mutation). The PAM2 mutation completely abolished the interaction with PABP, which was assessed using the GST-pulldown assay with zebrafish embryo lysates (Fig. 2*B*). In the tethering assay, the PAM2 mutation slightly reduced repression activity (Fig. 2 *C* and *D*, $p < 0.05$). Deadenylation of the Rluc-BoxB-poly(A) mRNA was still induced by the PAM2 mutant in this context (Fig. 2*E*). These results indicate that TNRC6 silencing activity is mediated by the PAM2 motif as suggested in the previous studies (18, 20), yet the contribution might not be predominant in zebrafish embryos.

To characterize repression activities that remained in the PAM2 mutant, we focused on the residues PPPGLT, which are located at the C terminus of the Mid domain and are highly conserved in the TNRC6 family proteins (hereafter referred to as the P-GL motif, Fig. 2*A*). A mutation introduced into this motif (G1544 and L1545 to A; P-GL mutation) did not affect PABP interaction (Fig. 2*B*). On the contrary, the P-GL mutation partially reduced the repression activity of the Mid domain ($p < 0.01$) with no obvious effect on deadenylation (Fig. 2 *C* and *E*, P-GL mut). Repression activity of the Mid domain was further impaired when the PAM2 and P-GL motifs were simultaneously mutated (Fig. 2*C*, PAM2/P-GL mut). Concomitantly, the deade-

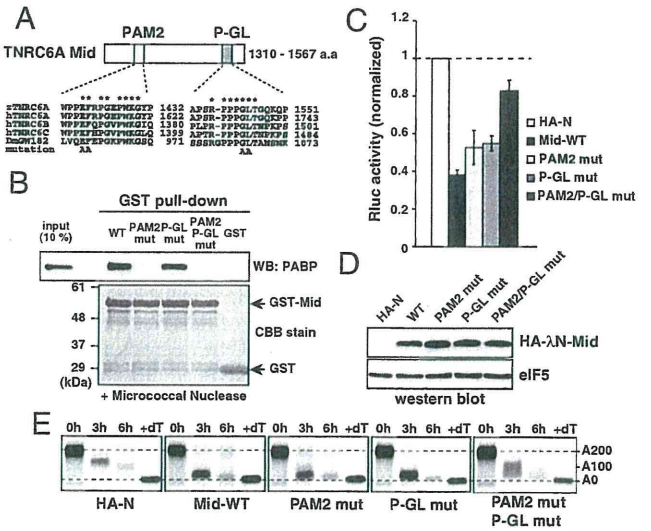

Fig. 2. The Mid domain of TNRC6A represses translation via two motifs. (*A*) Schematic representation of the Mid domain of zebrafish TNRC6A. The two conserved motifs (PAM2 and P-GL) are shown. Sequence alignments of each motif comparing zebrafish TNRC6A, human TNRC6 proteins, and fly GW182 are shown. Conserved residues are marked with asterisks. Alanine substitutions introduced in the current study are shown on the bottom. (*B*) GST-pulldown assay detecting interaction between the GST-Mid domain and zebrafish PABP. A total of 10% of embryonic lysate was loaded as an input. PABP was detected using Western blotting (*Upper*). GST fusion proteins were visualized using CBB stain (*Lower*). (*C*) The results of the tethering assay with TNRC6A Mid domain mutants. The data were collected and are shown as described in Fig. 1*C*. (*D*) Western blot detecting HA-λN-tagged Mid domain proteins. The membrane was probed with anti-eIF5 antibody as a control. (*E*) The poly(A) tail analysis of the injected Rluc-BoxB-pA reporter mRNA using RNaseH digestion and northern blot at 0, 3 and 6 hours. The lane +dT shows a completely deadenylated fragment (A0).

nylation activity was reduced in the double mutant (Fig. 2*E*). These results suggested that a previously undescribed P-GL motif in the Mid domain contributes to the translational inhibition in concert with the PAM2 motif.

To test the contributions of PAM2 and P-GL motifs in the context of full-length TNRC6A function, we performed two experiments. First, we introduced the mutations into the full-length TNRC6A and tested their effects in the tethering assay (Fig. S2 *A*–*C*). The simultaneous loss of both PAM2 and P-GL motifs, but not the loss of one of the two motifs, strongly impaired the repression activity of TNRC6A at translation level. Second, to test the activity of TNRC6A variants in the context of miRNA-mediated repression, we asked if exogenous TNRC6A variants enhance miR-430-mediated repression of the GFP sensor transgene (Fig. S2*D*; see Fig. 5 for detailed information of the GFP-miR-430 sensor). Overexpression of wild-type, PAM2 mutant, and P-GL mutant versions of TNRC6A promoted miR-430-mediated repression of the GFP-miR-430 sensor. In contrast, the double mutant failed to promote repression by miR-430 (Fig. S2 *E* and *F*). These two experiments indicated that our motif analysis with the Mid domain fragment well captured the actions of the full-length TNRC6A.

TNRC6A Mediates Translational Inhibition Independent of Deadenylation. Given the predominant contribution of the PAM2 and the P-GL motifs to translational inhibition with the moderate effect on deadenylation, we next asked if the translational inhibition induced by these two motifs was independent of deadenylation. To this end, we performed two experiments. First, we analyzed the physical interactions between the Mid domain and deadenylase components that have been implicated in miRNA-mediated deadenylation (18, 21, 23, 24). Consistent with its deadenylation activity in the tethering assay, the GST-Mid domain interacted with in vitro translated Myc-tagged PAN3 and CCR4/CAF1 but not with eIF4E (Fig. 3*A* and Fig. S3 *A* and *B*). Notably, the PAM2/P-GL double mutant still interacted with these factors with reduced affinity to PAN3. Second, we asked whether the Mid domain induced translational repression in the absence of deadenylation. To this end, we generated a synthetic poly(A) tail that contained a 98 nt poly(A) sequence followed by a 10 nt poly(C) sequence (A98C10, Fig. 3*B*). The A98C10 tail was not deadenylated by the Mid domain during the assay (Fig. 3*C*). On the other hand, the A98C10 tail enhanced Rluc expression similar to the normal poly(A) tail (Fig. S4*A*). Tethering experiments revealed that the Mid domain strongly silenced tethered mRNA with the A98C10 tail. Furthermore, the coordinated contribution of the PAM2 and P-GL motifs was observed with the A98C10 tail (Fig. 3*D*). These experiments showed that the Mid domain of TNRC6A inhibited translation via the PAM2 and P-GL motifs in a deadenylation-independent manner.

The PAM2 and P-GL Motifs Contribute to Translational Silencing Through Distinct Mechanisms. Next, we determined whether the PAM2 and P-GL motifs required PABP for their function in translation repression. To this end, we utilized Paip2 (PABP-interacting protein 2). Paip2 binds to PABP via its PAM1 and PAM2 motifs, and sequesters PABP by displacing it from the poly(A) tail and eIF4G (25). Hence, we predicted that the repression by the Mid domain would be diminished by Paip2 if PABP is the only molecular target for the Mid domain. First we confirmed that the A98C10 tail failed to stimulate translation in the presence of excess Paip2 (Fig. S4*B*). In the presence of excess Paip2, the Mid domain repressed translation of Rluc-BoxB-A98C10 mRNA (Fig. 3*E*). This result suggests that the Mid domain inhibits translation via a PABP-independent mechanism. Consistent with this idea, the Mid domain with the PAM2 mutation inhibited translation of Rluc-BoxB-A98C10 mRNA similar to the wild-type Mid domain ($p > 0.38$). In contrast, the P-GL mutation diminished

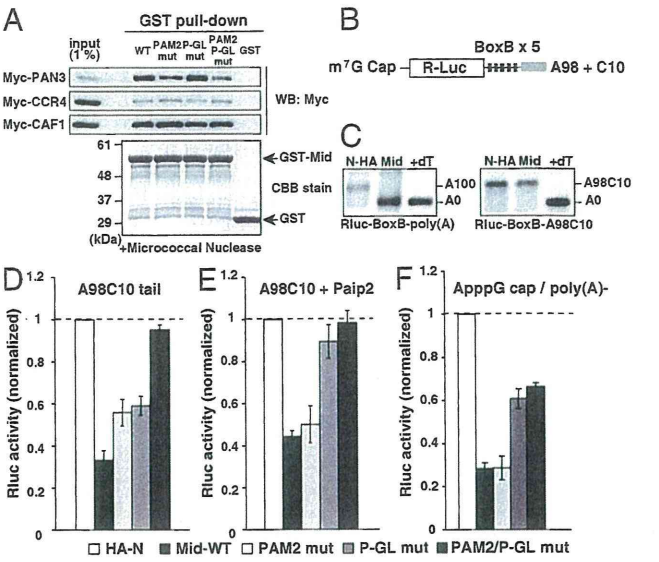

Fig. 3. The Mid domain of TNRC6A represses translation via deadenylation-independent mechanisms. (*A*) The GST-pulldown assay detecting interactions between the GST-Mid domain and deadenylase components translated in rabbit reticulocyte lysate. Total of 1% of in vitro translation reaction was loaded as an input. Myc-tagged proteins were detected using Western blotting (*Upper*). GST fusion proteins were visualized using CBB stain (*Lower*). (*B*) Rluc reporter mRNA containing 5 copies of BoxB sites followed by the A98C10 tail. (*C*) The poly(A) tail analysis of the Rluc-BoxB reporter mRNAs at six hours, in the presence of control HA-λN peptide (HA-N) or the HA-λN tagged Mid domain (Mid). *Left*: The reporter mRNA with a normal poly(A) tail [Rluc-BoxB-poly(A)]. *Right*: The reporter mRNA with an A98C10 tail (Rluc-BoxB-A98C10). The lane +dT shows a completely deadenylated fragment (A0). (*D*) Tethering assay of the TNRC6A Mid domain with reporter mRNA containing the A98C10 tail in the presence of Myc-GFP. (*E*) Tethering assay of the TNRC6A Mid domain with reporter mRNA containing the A98C10 tail in the presence of Myc-Paip2. (*F*) Tethering assay of the TNRC6A Mid domain constructs with a reporter mRNA containing the 5′ ApppG cap without a poly(A) tail. Graphs in *D*, *E*, and *F* show the averages of three independent experiments. Error bars show SD.

most of the repressive effect caused by the Mid domain in the presence of Paip2. Hence, the PAM2 motif required PABP for translational inhibition, while the P-GL motif did not. As an alternative approach, we determined whether the m^7G cap and the poly(A) tail, which are two important constituents for translation initiation, are required for translational inhibition by the Mid domain. Although the translation efficiency was significantly reduced in the absence of the m^7G cap and the poly(A) tail (Fig. S4*A*), the tethering assay revealed that the Mid domain repressed bound mRNA even in the absence of the m^7G cap and poly(A) tail (Fig. 3*F*). Analysis with Mid domain mutants showed that the P-GL motif, but not the PAM2 motif, contributed to repression of this reporter mRNA. The contribution of the P-GL motif was not attributed to the change in the RNA stability (Fig. S4*C*), indicating that the P-GL motif inhibited translation. These results strongly suggested that the Mid domain of TNRC6A inhibits translation through two distinct mechanisms.

Direct Translational Inhibition Is a Major Output of miRNA-Mediated Repression During Zebrafish Embryogenesis. To validate our findings obtained in the tethering assay, we designed a miRNA reporter system in zebrafish embryos using a firefly luciferase (Fluc) mRNA containing the 3′UTR of an endogenous miR-1 target gene, pdlim1 (26) (Fig. 4*A*). The Fluc-pdlim1 mRNA and a non-targeted mRNA encoding Renila luciferase (Rluc) were microinjected into fertilized eggs together with the miR-1 duplex or control miR-124 duplex. Six or 10 h after the injection, a luciferase assay and quantitative RT-PCR (qRT-PCR) were performed

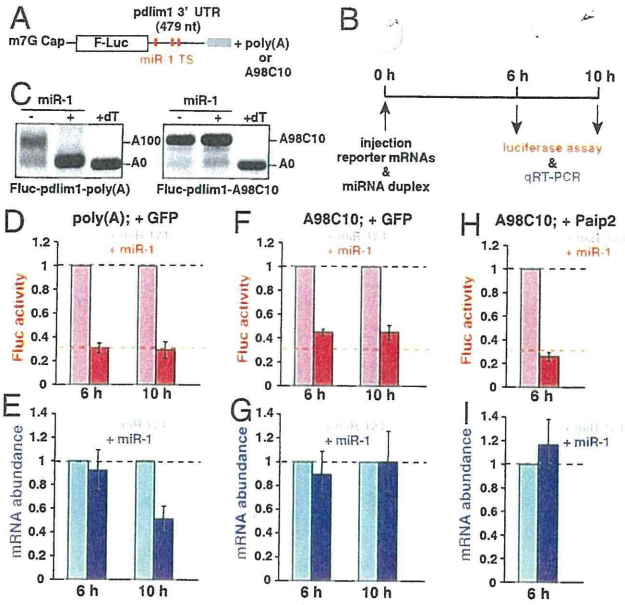

Fig. 4. miR-1 represses target mRNA in a deadenylation- and PABP-independent manner in zebrafish embryos. (*A*) Fluc reporter mRNA containing zebrafish pdlim1 3′UTR. Red boxes indicate the target site for miR-1. (*B*) Scheme of the miR-1 repression assay in zebrafish embryos. (*C*) The poly(A) tail analysis of the Fluc-pdlim1 3′UTR reporter mRNAs at six hours in the absence (–) or presence (+) of the miR-1 duplex. The left panel shows the reporter mRNA with a normal poly(A) tail [Fluc-pdlim1-poly(A)]. The right panel shows the reporter mRNA with the A98C10 tail (Fluc-pdlim1-A98C10). (*D* and *E*) The results of the miR-1 repression assay with reporter mRNA containing a normal poly(A) tail in the presence of control Myc-GFP. (*F* and *G*) Results of the miR-1 repression assay with reporter mRNA containing the A98C10 tail in the presence of control Myc-GFP. (*H* and *I*) Results of the miR-1 repression assay with reporter mRNA containing the A98C10 tail in the presence of Myc-Paip2. *D*, *F*, and *H* show normalized Fluc activity. *E*, *G*, and *I* show normalized Fluc mRNA levels, which were measured using qRT-PCR. The values of the experiments using miR-124 were set to one at each time point. The data shows averages of three independent experiments. Error bars show SD.

to measure protein expression and mRNA stability (Fig. 4*B*). As observed in the tethering assay, the A98C10 tail resisted deadenylation by miR-1 in this system (Fig. 4*C*).

The analysis using Fluc-pdlim1 mRNA with the normal poly (A) tail revealed strong repression of Fluc activity by miR-1 at 6 h (to approximately 30% compared to the miR-124 duplex), with no obvious change in mRNA abundance (Fig. 4 *D* and *E*, 6 h). Substantial mRNA degradation by miR-1 was detected at 10 h. However, miR-1-mediated mRNA reduction (approximately 50% compared to miR-124) does not fully account for the overall repressive effect of miR-1, which was measured by the luciferase activity (approximately 30%) (Fig. 4 *D* and *E*, 10 h). These results suggest a major contribution of translational inhibition in the miRNA pathway during zebrafish embryogenesis. To validate the contribution of deadenylation to miRNA-mediated repression, we performed the miR-1 repression assay with the deadenylation-resistant A98C10 tail. This analysis revealed two important findings. First, miR-1 inhibited translation of Fluc-pdlim1 mRNA with the A98C10 tail with a lower efficiency compared to the Fluc-pdlim1 mRNA with the normal poly(A) tail (approximately 45% with the A98C10 tail, versus approximately 30% with the normal poly(A) tail at 6 h; Fig. 4*F*). Second, the A98C10 tail inhibited miR-1-mediated Fluc mRNA degradation during the assay (Fig. 4*G*). These analyses confirmed a major contribution of deadenylation-independent translational inhibition during miRNA-mediated repression. Next, we analyzed the involvement of PABP-related mechanism in miRNA-mediated translational inhibition. Inhibition of PABP by Paip2 did not abrogate miR-1-mediated repression. Rather, it promoted miR-1-mediated translational inhibition of the Fluc-pdlim1-A98C10 mRNA to approximately 30% (Fig. 4 *H* and *I*). Hence, miR-1 can induce translation repression in parallel to the PABP inhibiton by Paip2. These results reveal distinct contributions of deadenylation, PABP inhibition, and PABP-independent translational inhibition to miRNA-mediated repression in vivo.

A PABP-Independent Mechanism of miRNA-Mediated Repression Operates During Zebrafish Embryogenesis. To further confirm whether miRNA inhibited its target mRNA via PABP-independent repression pathways in vivo, we depleted PABP from zebrafish embryos and analyzed the effects on miRNA-mediated repression. Among zebrafish orthologues of vertebrate PABP genes, the expression of two PABPC1 paralogues (pabpc1a and pabpc1b) and PABPC4 was detected during zebrafish embryogenesis (Fig. 5*A* and Fig. S5*A*). Although pabpc1a mRNA was ubiquitously expressed during development, the expression of pabpc1b and pabpc4 mRNAs was restricted to specific tissues at 24 h post fertilization (hpf). Injection with the translation-blocking morpholino oligo (MO) for pabpc1a mRNA at the one-cell stage reduced total PABP levels to <1% compared to the injection of embryos with control MO (Fig. 5*B* and Fig. S5*B*; note that the antibody we used detected all three PABP proteins described above). Concomitantly, PABP-depleted embryos showed reduced formation of polysomes (Fig. 5*C*) and strong morphological defects (Fig. 5*D*, upper panels) at 24 hpf. Therefore, cellular PABP was reduced to nonfunctional levels in pabpc1a MO-injected embryos.

To monitor endogenous miRNA-mediated repression, we generated a transgenic zebrafish that ubiquitously expressed GFP mRNA containing three copies of the miR-430 target site (TS) [Tg(βactin-GFP-3xTS-miR-430)]. Expression of GFP protein from this reporter gene was strongly repressed throughout the embryo by the ubiquitous miRNA miR-430 in a target-site dependent manner (Fig. 5*D*, middle panels) (9, 27). Notably, miR-430 repressed the GFP reporter in PABP-depleted embryos. In situ hybridization revealed concomitant degradation of the reporter mRNA (Fig. 5*D*, lower panels), indicating that the repressive effect we observed in the transgenic embryos might be a combined output of initial translational repression and subsequent mRNA degradation. Similar findings were observed with another GFP transgenic line that visualized repression by muscle specific miRNA miR-1/206 (26) (Fig. S6). The PABP-depletion did not cause shortening of the basal poly(A) tail length as a secondary effect (Fig. 5*F*). These results with the transgenic lines, together with the results with injected reporter mRNAs in Fig. 4, show that miRNA silences its target mRNA via PABP-independent mechanism(s) during zebrafish embryogenesis.

Discussion

Due to its intricate outputs, it has been difficult to delineate the direct and primary consequence of miRNA-mediated repression (3, 11). In this study, we addressed a causal relationship between miRNA-mediated translational repression and deadenylation using three different approaches. First, we revealed that the PAM2 and P-GL motifs in the Mid domain of zebrafish TNRC6A induced translational inhibition in a deadenylation-independent manner (Figs. 2*C* and 3*D*). Second, we found that the Mid domain carrying the PAM2 and P-GL mutations showed reduced affinity to PAN3 but still interacted with CCR4/CAF1 deadenylases (Fig. 3*A* and Fig. S3 *A* and *B*). Third, miR-1 induced translational repression of its target reporter mRNA even in the absence of deadenylation (Fig. 4*F*). These observations collectively indicate that miRNA-mediated translational inhibition and deadenylation are independent outputs mediated through distinct molecular actions of TNRC6.

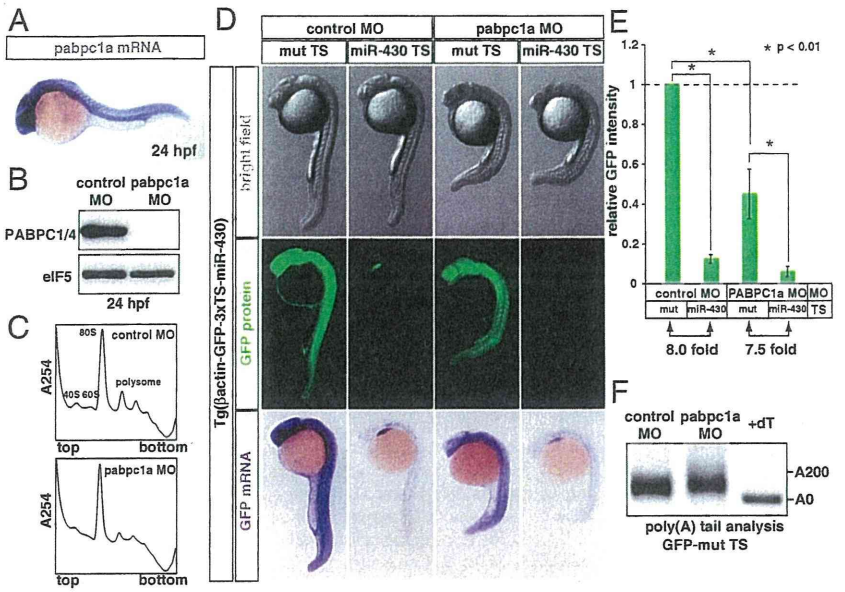

Fig. 5. miR-430 represses its target mRNA in the absence of PABP during zebrafish embryogenesis. (*A*) In situ hybridization detecting pabpc1a mRNA in a 24 hpf zebrafish embryo (purple). (*B*) Western blot detecting PABP protein in 24 hpf embryos injected with control MO or pabpc1a MO. The membrane was probed with anti-eIF5 antibody as a control. (*C*) The polysome profiles of control MO-injected (*Upper*) and pabpc1 MO-injected (*Lower*) zebrafish embryos at 24 hpf. (*D*) Analysis of miRNA-mediated target mRNA repression in the presence or absence of PABP. Bright field view (*Upper* panels), GFP fluorescence (*Middle* panels; green) and GFP mRNA (*Bottom* panels; purple) of 24 hpf zebrafish embryos expressing the GFP transgene with three copies of the imperfect target site for the ubiquitously expressed miRNA, miR-430 (miR-430 TS) or with mutated target sites (mut TS). Control MO (left columns) or pabpc1a MO (right columns) was injected as indicated. (*E*) Quantification of GFP expression levels in Fig. 5*D*. GFP intensity of the embryos with the mut TS and the control MO was set to one. Error bars show SD. Asterisks indicate $p < 0.01$ compared to the experiment with the mut TS and control MO. (*F*) The poly(A) tail analysis of the GFP mut TS mRNA with the control MO or pabpc1a MO. The lane +dT shows a completely deadenylated fragment (A0).

The use of the deadenylation-resistant A98C10 tail allowed us to determine the relative contributions of direct translational inhibition and deadenylation in the miRNA pathway. Although we observed the contribution of deadenylation to miR-1-mediated translational inhibition, we also observed substantial translational inhibition in the absence of deadenylation with miR-1 and the tethered Mid domain (Figs. 3*D* and 4*F*). These observations establish that translational inhibition by miRNA is not a mere consequence of deadenylation. Consistent with these findings, mRNAs that were translated in a poly(A) tail-independent manner were repressed by miRNA (10, 21). Hence, we propose that deadenylation plays an auxiliary role in the miRNA-mediated repression by consolidating translational inhibition, possibly through displacement of PABP from mRNA. We also observed that miRNA required deadenylation for target mRNA degradation that occurred at a later time point (Fig. 4*E*, 10 h). Therefore, we do not exclude the possibility that deadenylation and subsequent mRNA degradation play more active roles in miRNA-mediated silencing after extended periods, which has been suggested by previous genome-wide analyses (6–8). Nevertheless, a rapid and strong translational inhibition in our zebrafish system supported a model in which direct translational inhibition is central to miRNA-mediated gene silencing at early time points.

The mechanisms that mediate direct translational repression by miRNA have not been well characterized. Some of our data are consistent with a model in which miRNA/TNRC6 induces silencing by interacting with PABP via its PAM2 motif (11). In our tethering assay, the PAM2 motif in the Mid domain of zebrafish TNRC6A contributed to translational inhibition when PABP was involved in translation (Fig. 2*C*). This contribution was deadenylation-independent (Fig. 3*D*), indicating that the PAM2 motif contributed to translational inhibition by counteracting the function of PABP in translation. These observations are also consistent with previous studies arguing that miRNA targets the m^7G cap-dependent translation initiation process (28–31). In addition, our study indicated that the PAM2–PABP interaction was not the only mechanism used by miRISC to inhibit translation. First, the mutation into the PAM2 motif only weakly reduced the repression activity of the Mid domain (Figs. 2 and 3) and the full-length TNRC6A (Fig. S2). Second, miR-1 and the Mid domain induced translational inhibition even in a PABP-independent manner (Figs. 3*E* and 4*F*). Third, depletion of PABP from zebrafish embryos allowed endogenous miRNAs to silence their target mRNAs (Fig. 5 and Fig. S6). Hence, zebrafish miRISC is equipped with a mechanism that does not require PABP for target mRNA silencing. In contrast, previous studies in mammalian cultured cells have shown correlations between cellular PABP activity and miRNA-mediated repression (20, 32). It is therefore possible that the contribution of the PAM2–PABP interaction to miRNA-mediated repression is conditional on the general translation status in the cell.

We identified a previously undescribed conserved motif, the P-GL motif, which was within the Mid domain of TNRC6A, as a PABP-independent translation repression mechanism. The action of the P-GL motif was clearly distinct from that of the PAM2 motif in three aspects. First, the P-GL motif was not involved in PABP binding (Fig. 2*B*). Second, the P-GL motif contributed to translational repression irrespective of the presence of poly(A) tail or the PABP activity (Figs. 3*E* and *F*). Third, the P-GL motif contributed to the repression of mRNA with the unnatural 5′ ApppG cap structure (Fig. 3*F*). Hence, the P-GL motif repressed mRNA translation independent of essential constituents of the canonical translation initiation pathway. Because the use of the ApppG cap structure significantly reduced the basal translation activity (Fig. S4*A*), the exact contribution and the molecular basis of the observed repression activity need to be interpreted in the context of the m^7G capped and polyadenylated mRNA. Nevertheless, it is worth noticing that the cap-independent repression activity observed with the P-GL motif is consistent with post-initiation repression models of miRNA (33–36). Based on these observations, we propose a "double lock model" of miRNA-mediated translational repression, in which miRNA inhibits two distinct translation steps through TNRC6 (Fig. S7).

While this manuscript was under revision, three papers reported additional functional motifs in fly GW182 and mammalian TNRC6 proteins that mediate binding to the CCR4/NOT1 and PAN2/PAN3 deadenylase complexes (37–39). Interestingly, those complexes induced repression not only via deadenylation but also via deadenylation-independent mechanism(s) (37, 39). Moreover, Fukaya and Tomari recently reported that, consistent with our findings in zebrafish, miRNA induces translation repression independent of deadenylation and PABP in the fly in vitro system (40). Although the relative contributions of these pathways need to be clarified, our current study and these recent reports collec-

tively indicate that miRNA system utilizes multiple redundant mechanisms to silence target mRNAs. The characterization of multiple translational inhibition activities of TNRC6 proteins in a wide variety of experimental systems may reconcile contradicting observations on miRNA-mediated translational inhibition (3, 11). It is tempting to speculate that, by having multiple repression mechanisms, miRNA performs robust control of target gene expression under diverse cellular contexts.

Materials and Methods

Tethering Assay in Zebrafish Embryos. The mRNAs were transcribed using an mMessage mMachine SP6 kit (Ambion). ApppG capped mRNA was synthesized in the presence of an ApppG cap analogue (New England Biolabs) instead of an m^7GpppG cap analogue. To add a normal poly(A) tail, the mRNA was polyadenylated in vitro using a poly(A) tailing kit (Ambion). For poly(A)- mRNA, we injected a MO that binds to the end of the mRNA to inhibit polyadenylation (TB-MO). For mRNA injections, Rluc mRNA and Fluc mRNA were diluted to a final concentration of 50 ng/μL each. Effector mRNAs were diluted to obtain solutions with equimolar concentrations of effector mRNA. HA-λN-Mid mRNA was diluted to a final concentration of 100 ng/μL. The mRNA encoding myc-tagged GFP or zebrafish Paip2 was added to a final concentration of 200 ng/μL. Approximately 1,000 pl of solution containing reporter mRNAs and effecter mRNAs was injected into one-cell stage zebrafish embryos. A total of 5–10 embryos were collected at the shield stage (6 hpf) and lysed in Passive lysis buffer (Promega). The luciferase activities were measured using the Dual-Luciferase Reporter assay system and GloMax 20/20 n luminometer (Promega). Rluc activity intensity (IRluc) was normalized to the intensity of Fluc activity (IFluc). The normalized Rluc activity for each experiment with HA-N effector encoding XX was calculated as follows. Fold change = (IFluc + HA-N-XX/IRluc + HA-N-XX)/(IFluc-control/IRluc-control). The values obtained using HA-N empty mRNA were used for controls. Each sample was measured as three replicates. The p value was calculated using Student's t test.

qRT-PCR. A total of five embryos were retained after each injection experiment, and total RNA was extracted by ISOGEN (Nippon gene). The cDNA was synthesized using the PrimeScript RT reagent kit (TAKARA). A random hexamer was used for cDNA synthesis to avoid detecting differences in the poly(A) tail length. To assess Fluc mRNA and Rluc mRNA levels, qRT-PCR was performed with SYBR Premix EX Taq II and the Thermal Cycler Dice Real Time System (TAKARA) following a standard protocol. Specific amplification of the PCR products was confirmed by analyzing the dissociation curve, running the products on an agarose gel, and sequencing. Each sample was measured as duplicates, and each experiment was repeated three times.

Additional materials and methods are described in *SI Text*.

ACKNOWLEDGMENTS. We thank Y. Tomari and M. W. Hentze for discussions and helpful comments on our project. We are also grateful to N. Sonenberg, M. R. Fabian, A. J. Giraldez, T. Inada, and M. Wakiyama for discussions; C. B. Chien and K. Kawakami for Tol2 constructs; and A. Kulozik for λN tethering constructs. We thank H. Fukaki and T. Goh for their help in qRT-PCR; K. Fukumura and D. Cifuentes for their critical comments on the manuscript; Y. Takeda for cloning zebrafish PABPC1a and Paip2; R. Kusakabe for sharing miR1/206 MOs; S. Kanamura for fish maintenance; and members of our laboratory for their support. This work was supported by Grants-in-Aid for Scientific Research from Japan Ministry of Education, Culture, Sports, Science and Technology to Y.M (22115510) and K.I (20112003), the Uehara Memorial Foundation and the Senri Life Science Foundation to Y.M, and the Asahi Glass Foundation to K.I. A.F. is a research fellow of the Japan Society for the Promotion of Science.

1. Bushati N, Cohen SM (2007) microRNA functions. *Annu Rev Cell Dev Biol* 23:175–205.
2. Bartel DP (2009) MicroRNAs: Target recognition and regulatory functions. *Cell* 136:215–233.
3. Fabian MR, Sonenberg N, Filipowicz W (2010) Regulation of mRNA translation and stability by microRNAs. *Annu Rev Biochem* 79:351–379.
4. Lim LP, et al. (2005) Microarray analysis shows that some microRNAs downregulate large numbers of target mRNAs. *Nature* 433:769–773.
5. Giraldez AJ, et al. (2006) Zebrafish MiR-430 promotes deadenylation and clearance of maternal mRNAs. *Science* 312:75–79.
6. Guo H, Ingolia NT, Weissman JS, Bartel DP (2010) Mammalian microRNAs predominantly act to decrease target mRNA levels. *Nature* 466:835–840.
7. Hendrickson DG, et al. (2009) Concordant regulation of translation and mRNA abundance for hundreds of targets of a human microRNA. *PLoS Biol* 7:e1000238.
8. Selbach M, et al. (2008) Widespread changes in protein synthesis induced by microRNAs. *Nature* 455:58–63.
9. Mishima Y, et al. (2006) Differential regulation of germline mRNAs in soma and germ cells by zebrafish miR-430. *Curr Biol* 16:2135–2142.
10. Wu L, Fan J, Belasco JG (2006) MicroRNAs direct rapid deadenylation of mRNA. *Proc Natl Acad Sci USA* 103:4034–4039.
11. Huntzinger E, Izaurralde E (2011) Gene silencing by microRNAs: contributions of translational repression and mRNA decay. *Nat Rev Genet* 12:99–110.
12. Hutvagner G, Simard MJ (2008) Argonaute proteins: Key players in RNA silencing. *Nat Rev Mol Cell Biol* 9:22–32.
13. Eulalio A, Tritschler F, Izaurralde E (2009) The GW182 protein family in animal cells: New insights into domains required for miRNA-mediated gene silencing. *RNA* 15:1433–1142.
14. Behm-Ansmant I, et al. (2006) mRNA degradation by miRNAs and GW182 requires both CCR4:NOT deadenylase and DCP1:DCP2 decapping complexes. *Genes Dev* 20:1885–1898.
15. Till S, et al. (2007) A conserved motif in Argonaute-interacting proteins mediates functional interactions through the Argonaute PIWI domain. *Nat Struct Mol Biol* 14:897–903.
16. Eulalio A, Helms S, Fritzsch C, Fauser M, Izaurralde E (2009) A C-terminal silencing domain in GW182 is essential for miRNA function. *RNA* 15:1067–1077.
17. Lazzaretti D, Tournier I, Izaurralde E (2009) The C-terminal domains of human TNRC6A, TNRC6B, and TNRC6C silence bound transcripts independently of Argonaute proteins. *RNA* 15:1059–1066.
18. Fabian MR, et al. (2009) Mammalian miRNA RISC recruits CAF1 and PABP to affect PABP-dependent deadenylation. *Mol Cell* 35:868–880.
19. Jinek M, Fabian MR, Coyle SM, Sonenberg N, Doudna JA (2010) Structural insights into the human GW182-PABC interaction in microRNA-mediated deadenylation. *Nat Struct Mol Biol* 17:238–240.
20. Huntzinger E, Braun JE, Heimstadt S, Zekri L, Izaurralde E (2010) Two PABPC1-binding sites in GW182 proteins promote miRNA-mediated gene silencing. *EMBO J* 29:4146–4160.
21. Eulalio A, et al. (2009) Deadenylation is a widespread effect of miRNA regulation. *RNA* 15:21–32.
22. Zipprich JT, Bhattacharyya S, Mathys H, Filipowicz W (2009) Importance of the C-terminal domain of the human GW182 protein TNRC6C for translational repression. *RNA* 15:781–793.
23. Piao X, Zhang X, Wu L, Belasco JG (2010) CCR4-NOT deadenylates mRNA associated with RNA-induced silencing complexes in human cells. *Mol Cell Biol* 30:1486–1494.
24. Chen CY, Zheng D, Xia Z, Shyu AB (2009) Ago-TNRC6 triggers microRNA-mediated decay by promoting two deadenylation steps. *Nat Struct Mol Biol* 16:1160–1166.
25. Sonenberg N, Dever TE (2003) Eukaryotic translation initiation factors and regulators. *Curr Opin Struct Biol* 13:56–63.
26. Mishima Y, et al. (2009) Zebrafish miR-1 and miR-133 shape muscle gene expression and regulate sarcomeric actin organization. *Genes Dev* 23:619–632.
27. Giraldez AJ, et al. (2005) MicroRNAs regulate brain morphogenesis in zebrafish. *Science* 308:833–838.
28. Pillai RS, et al. (2005) Inhibition of translational initiation by Let-7 MicroRNA in human cells. *Science* 309:1573–1576.
29. Humphreys DT, Westman BJ, Martin DI, Preiss T (2005) MicroRNAs control translation initiation by inhibiting eukaryotic initiation factor 4E/cap and poly(A) tail function. *Proc Natl Acad Sci USA* 102:16961–16966.
30. Mathonnet G, et al. (2007) MicroRNA inhibition of translation initiation in vitro by targeting the cap-binding complex eIF4F. *Science* 317:1764–1767.
31. Thermann R, Hentze MW (2007) Drosophila miR2 induces pseudo-polysomes and inhibits translation initiation. *Nature* 447:875–878.
32. Walters RW, Bradrick SS, Gromeier M (2010) Poly(A)-binding protein modulates mRNA susceptibility to cap-dependent miRNA-mediated repression. *RNA* 16:239–250.
33. Olsen PH, Ambros V (1999) The lin-4 regulatory RNA controls developmental timing in Caenorhabditis elegans by blocking LIN-14 protein synthesis after the initiation of translation. *Dev Biol* 216:671–680.
34. Wang B, Yanez A, Novina CD (2008) MicroRNA-repressed mRNAs contain 40S but not 60S components. *Proc Natl Acad Sci USA* 105:5343–5348.
35. Petersen CP, Bordeleau ME, Pelletier J, Sharp PA (2006) Short RNAs repress translation after initiation in mammalian cells. *Mol Cell* 21:533–542.
36. Nottrott S, Simard MJ, Richter JD (2006) Human let-7a miRNA blocks protein production on actively translating polyribosomes. *Nat Struct Mol Biol* 13:1108–1114.
37. Braun JE, Huntzinger E, Fauser M, Izaurralde E (2011) GW182 proteins directly recruit cytoplasmic deadenylase complexes to miRNA targets. *Mol Cell* 44:120–133.
38. Fabian MR, et al. (2011) miRNA-mediated deadenylation is orchestrated by GW182 through two conserved motifs that interact with CCR4-NOT. *Nat Struct Mol Biol* 18:1211–1217.
39. Chekulaeva M, et al. (2011) miRNA repression involves GW182-mediated recruitment of CCR4-NOT through conserved W-containing motifs. *Nat Struct Mol Biol* 18:1218–1226.
40. Fukaya T, Tomari Y (2011) PABP is not essential for microRNA-mediated translational repression and deadenylation in vitro. *EMBO J*, 10.1038/emboj.2011.426.